iScience

CellPress

Article

CIP2A Constrains Th17 Differentiation by Modulating STAT3 Signaling

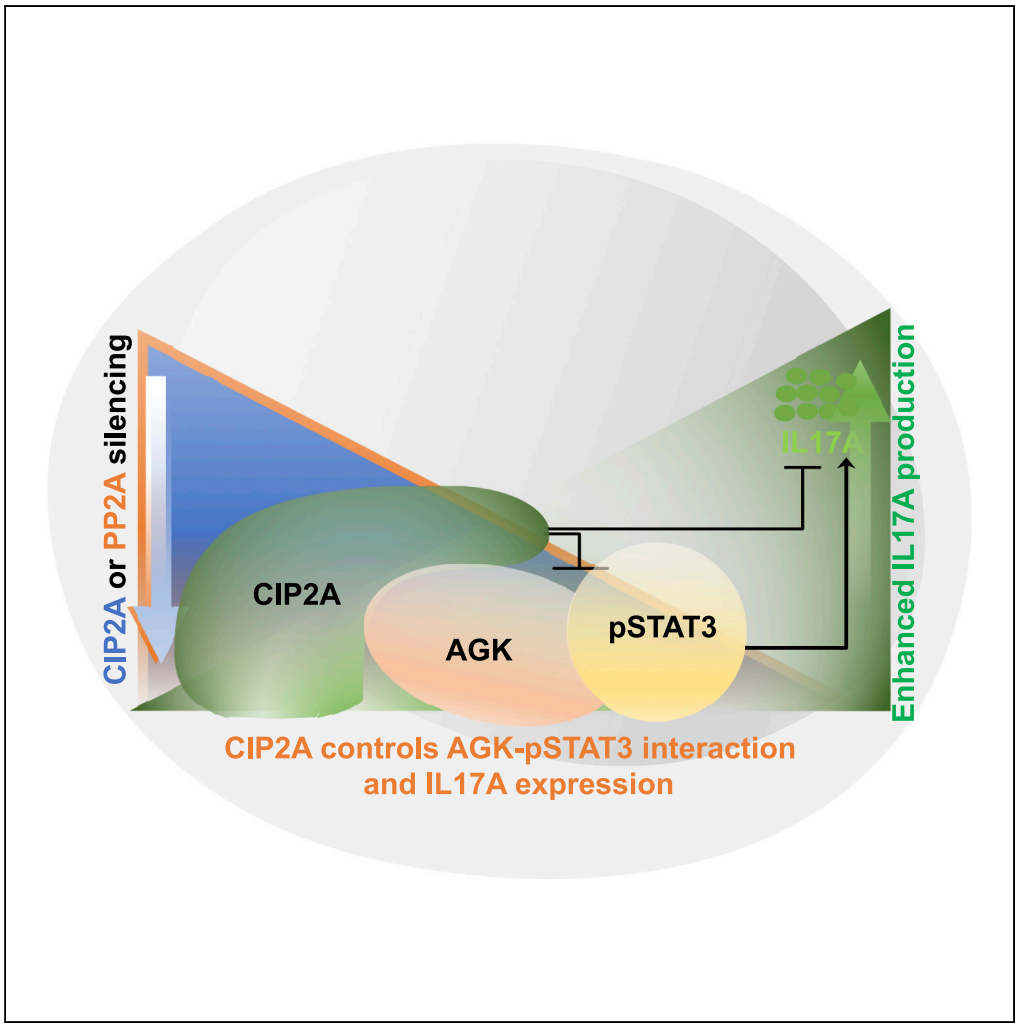

Mohd Moin Khan, Ubaid Ullah, Meraj H. Khan, ..., Laura L. Elo, Jukka Westermarck, Riitta Lahesmaa

rilahes@utu.fi

HIGHLIGHTS

CIP2A deficiency leads to increased IL-17 production by Th17 cells

STAT3 phosphorylation is increased and prolonged in CIP2A-deficient Th17 cells

Mass spectrometry-based analysis of pSTAT3 interactome

CIP2A regulates interaction between acylglycerol kinase (AGK) and pSTAT3

DATA AND CODE AVAILABILITY

GSE118094

Khan et al., iScience *23*, 100947
March 27, 2020
https://doi.org/10.1016/j.isci.2020.100947

iScience

CellPress

Article

CIP2A Constrains Th17 Differentiation by Modulating STAT3 Signaling

Mohd Moin Khan,[1,2] Ubaid Ullah,[1] Meraj H. Khan,[1] Lingjia Kong,[1,3,4] Robert Moulder,[1] Tommi Välikangas,[1,5] Santosh Dilip Bhosale,[1] Elina Komsi,[1] Omid Rasool,[1] Zhi Chen,[1,7] Laura L. Elo,[1] Jukka Westermarck,[1,6] and Riitta Lahesmaa[1,8,*]

SUMMARY

Cancerous Inhibitor of Protein Phosphatase 2A (CIP2A) is an oncogene and a potential cancer therapy target protein. Accordingly, a better understanding of the physiological function of CIP2A, especially in the context of immune cells, is a prerequisite for its exploitation in cancer therapy. Here, we report that CIP2A negatively regulates interleukin (IL)-17 production by Th17 cells in human and mouse. Interestingly, concomitant with increased IL-17 production, CIP2A-deficient Th17 cells had increased strength and duration of STAT3 phosphorylation. We analyzed the interactome of phosphorylated STAT3 in CIP2A-deficient and CIP2A-sufficient Th17 cells and indicated together with genome-wide gene expression profiling, a role of Acylglycerol Kinase (AGK) in the regulation of Th17 differentiation by CIP2A. We demonstrated that CIP2A regulates the strength of the interaction between AGK and STAT3, and thereby modulates STAT3 phosphorylation and expression of IL-17 in Th17 cells.

INTRODUCTION

Cancerous Inhibitor of Protein Phosphatase 2A (CIP2A) was first characterized as a modulator of activity of Protein Phosphatase 2A (PP2A) toward serine-62 phosphorylated MYC, leading to stabilization of the MYC protein (Junttila et al., 2007). The oncogenic nature of CIP2A was later confirmed in various human malignancies (Kauko and Westermarck, 2018) making it a promising target for cancer therapy (Junttila et al., 2007; Janghorban et al., 2014; Lucas et al., 2016). Mechanistically, the oncogenic activity of CIP2A can be explained by its activity toward the tumor suppressive PP2A B-subunit B56 and presumed effects in selectively inhibiting PP2A/B56 substrate recognition (Wang et al., 2017). In addition to cancer, increased CIP2A levels have also been detected in the neurons of patients with Alzheimer disease (AD) leading to increased phosphorylation of Tau protein, suggesting CIP2A also to be a potential therapeutic target for AD (Shentu et al., 2018). Although CIP2A is associated with these disease states, there is a need for a better understanding of its role in normal cellular physiology. Its expression has also been associated with autophagy and increased cell proliferation (Yu et al., 2013). It promotes cell cycle progression, premature chromosome segregation, and aneuploidy (Pallai et al., 2015). We have previously demonstrated that CIP2A deficiency results in defects in T cell activation (Côme et al., 2016); however, nothing is known with respect to the function of CIP2A in the differentiation of different T helper (Th) cell subsets.

Interleukin 17 (IL-17)-producing Th17 cells protect the mucosal surfaces and play a crucial role in host defense against pathogens, such as fungi and extracellular bacteria (Gaffen et al., 2011; Romani, 2011). Dysregulated Th17 differentiation leads to several autoimmune and inflammatory pathologies, including psoriasis, rheumatoid arthritis (RA), multiple sclerosis, and inflammatory bowel disease (Kleinewietfeld and Hafler, 2013; Kleinewietfeld et al., 2013; Wu et al., 2013; Yosef et al., 2013; Lee et al., 2014; Meyer Zu Horste et al., 2016). Strategies to limit excessive Th17 response are therefore an attractive target to prevent Th17-mediated pathologies. Notably, the suppression of the activity of transcription factors (TF) driving Th17 differentiation, such as RORγt, has demonstrated impressive efficacy in preclinical disease models (Huh et al., 2011; Xu et al., 2011; Xiao et al., 2014). Moreover, inhibition of IL-17 by neutralizing antibodies has shown remarkable effectiveness in clinical trials in the pathology of several autoimmune diseases, such as psoriasis, ankylosing spondylitis, and multiple sclerosis (Robinson et al., 2013; Lønnberg et al., 2014). A better understanding of how Th17 cells function and their differentiation is regulated would facilitate the development of novel approaches to treat autoimmune diseases and other Th17 cell-mediated disorders.

[1]Turku Bioscience Centre, University of Turku and Åbo Akademi University, Tykistökatu 6A, Turku, Finland

[2]Turku Doctoral Programme of Molecular Medicine (TuDMM), University of Turku, Turku, Finland

[3]The Broad Institute of MIT and Harvard, Cambridge, USA

[4]Center for Computational and Integrative Biology, Massachusetts General Hospital, Boston, USA

[5]Doctoral Programme in Mathematics and Computer Sciences (MATTI), University of Turku, Turku, Finland

[6]Institute of Biomedicine, University of Turku, Turku, Finland

[7]Faculty of Biochemistry and Molecular Medicine, University of Oulu

[8]Lead Contact

*Correspondence: rilahes@utu.fi

https://doi.org/10.1016/j.isci.2020.100947

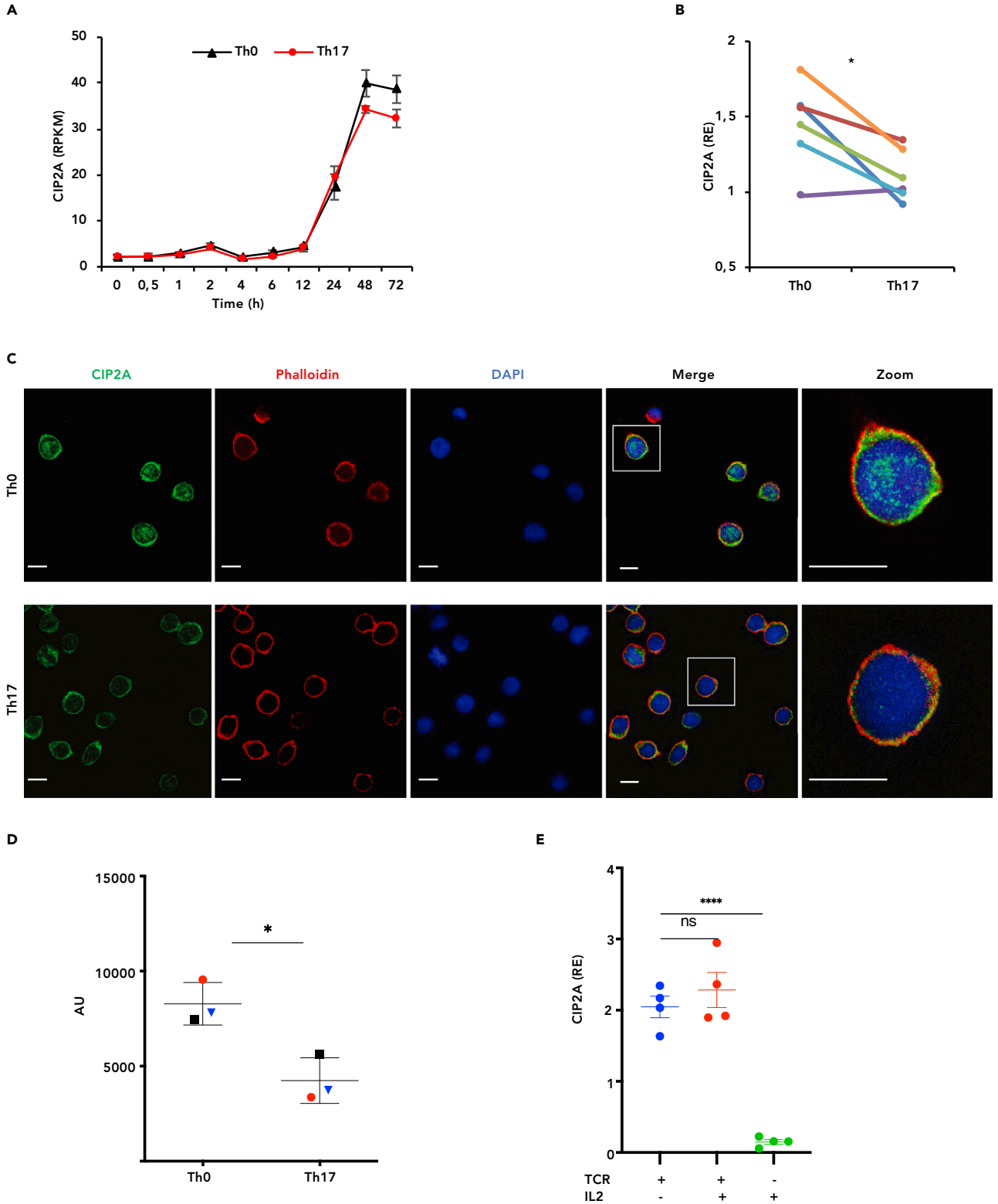

Figure 1. CIP2A Is Downregulated in Th17 Cells

(A) Expression profiles of CIP2A from human activated T cells (Th0) and Th17 cells at the indicated time points post cell activation (RNA-seq data from Tuomela et al. (2016)).

Figure 1. *Continued*

(B) Pairwise TaqMan qRT-PCR analysis of CIP2A expression at 24 h in Th0 and Th17 cells. The significance was determined using unpaired two-tailed t test; *$p < 0.05$.

(C) Confocal microscopic images of CIP2A staining in Th0 (top) and Th17 (bottom) cells (72 h). Scale bar, 7 μm.

(D) Statistical analysis of the confocal microscopy (C). The dot plot shows average corrected total cell fluorescence displayed as arbitrary unit (AU); each dot represents an independent experiment where 50–60 cells were analyzed. The analyses were performed using GraphPad Prism version 7.0d for Mac OS X (GraphPad Software), and the significance was determined using unpaired two-tailed t test; *$p < 0.05$.

(E) CIP2A expression analysis by TaqMan qRT-PCR in human T cells at 72 h after stimulation by TCR, IL-2, or both. Data were calculated as dCT values normalized with the housekeeping gene (EF1-alpha) and plotted as 2^{-dCt}. ****$p < 0.0001$ (Student's two-tailed unpaired t test). In all figures, the error bars represent the standard error of the mean. RE and AU stand for relative expression and arbitrary unit, respectively.

In the present study, we demonstrated that CIP2A silencing results in a significant increase in IL-17 production in human and mouse Th17 cells. Genome-wide profiling of gene expression in human CIP2A-silenced Th17 cells confirmed the upregulation of many Th17 cell-specific genes, including RORC and MAF. Concomitant with increased IL-17 production, we observed enhanced STAT3 (Y705) phosphorylation in CIP2A-deficient Th17 cells. To identify candidates responsible for enhanced STAT3 phosphorylation, we used a mass spectrometry (MS) (liquid chromatography [LC]-tandem MS [MS/MS])-based proteomics approach to study the interactome of phosphorylated (pSTAT3) in CIP2A-silenced and control Th17 cells. We demonstrated significantly increased interaction between acylglycerol kinase (AGK) and pSTAT3 under CIP2A-deficient condition that in turn may lead to enhanced STAT3 phosphorylation and IL-17 secretion in CIP2A-silenced Th17 cells. Notably, both inhibition of CIP2A and direct inhibition of PP2A catalytic subunit led to enhanced IL-17 expression in Th17 cells. This suggests that CIP2A negatively regulates human Th17 cell differentiation without inhibiting catalytic activity of PP2A complex.

RESULTS

CIP2A Is Downregulated in TH17 Cells

CIP2A is induced upon T cell activation, and its mRNA expression is reduced in Th17 cells (Figures 1A and 1B). Interestingly, in other CD4+ T cell subsets, there was no difference in the expression of CIP2A (Figures S1A and S1B) (Kanduri et al., 2015; Ubaid Ullah et al., 2018). We further confirmed reduced CIP2A expression in Th17 cells at the protein level (72 h) using confocal microscopy (Figures 1C and 1D). CIP2A localization by confocal microscopy suggested similar CIP2A expression in the nuclear and cytoplasmic fractions of Th0 and Th17 cells. Thus, reduced expression of CIP2A is not due to its altered localization in Th17 cells (Khan et al., 2020). On account of the early expression of *IL2* in response to T cell receptor (TCR) triggering/activation and its role in immune system, we sought to investigate whether the expression of CIP2A was regulated directly by TCR or through activation-induced autocrine/paracrine IL-2. Naive human CD4+ T cells were stimulated with either TCR or IL-2 alone or in combination for 72 h followed by measuring CIP2A expression by TaqMan qRT-PCR. Although TCR by itself was sufficient to induce the expression, stimulation with IL-2 alone did not result in any detectable expression of CIP2A (Figure 1E). Together, these results indicate that CIP2A is induced in T cells upon TCR triggering and is downregulated in Th17 cells.

CIP2A Negatively Regulates TH17 Differentiation

To determine the functional role of CIP2A in human CD4+ T cells, CIP2A was silenced using three different small interfering RNAs (siRNAs), each targeting different regions of the transcript. CIP2A expression was efficiently silenced both at protein and RNA levels by these three (siCIP2A1, siCIP2A4, and siCIP2A5) siRNAs (Figures 2A and 2B). In mouse, CIP2A was depleted using gene trap technology, as previously described (Ventelä et al., 2012). CIP2A homozygous mice ($CIP2A^{HOZ}$) were viable with normal lifespan and had strong depletion (more than 90%) of CIP2A expression when compared with CIP2A wild-type ($CIP2A^{WT}$) animals. In our earlier study, we reported reduced expression of CD69, a marker for activated T cells, in CIP2A-deficient human and mouse T cells in response to TCR activation (Côme et al., 2016). In the current study, we tested the effect of CIP2A silencing on IL2RA (CD25) expression, as IL2RA is another key receptor induced upon T cell activation. Like CD69, CD25 expression was also significantly downregulated in cells deficient in CIP2A (Figures S2A and S2B), further supporting the role of CIP2A in T cell activation.

CIP2A siRNA (siCIP2A) and non-targeting control siRNA (siNT) transfected human naive CD4+ T cells were differentiated toward the Th17 direction, and CCR6 surface expression and IL-17 levels were measured at 72 h. A significant increase in CCR6 expression (Figure 2C) and enhanced IL-17A expression, both at RNA (Figure 2D) and protein levels (Figure 2E), were observed in the CIP2A-silenced Th17 cells. To study if the effect of CIP2A on IL-17

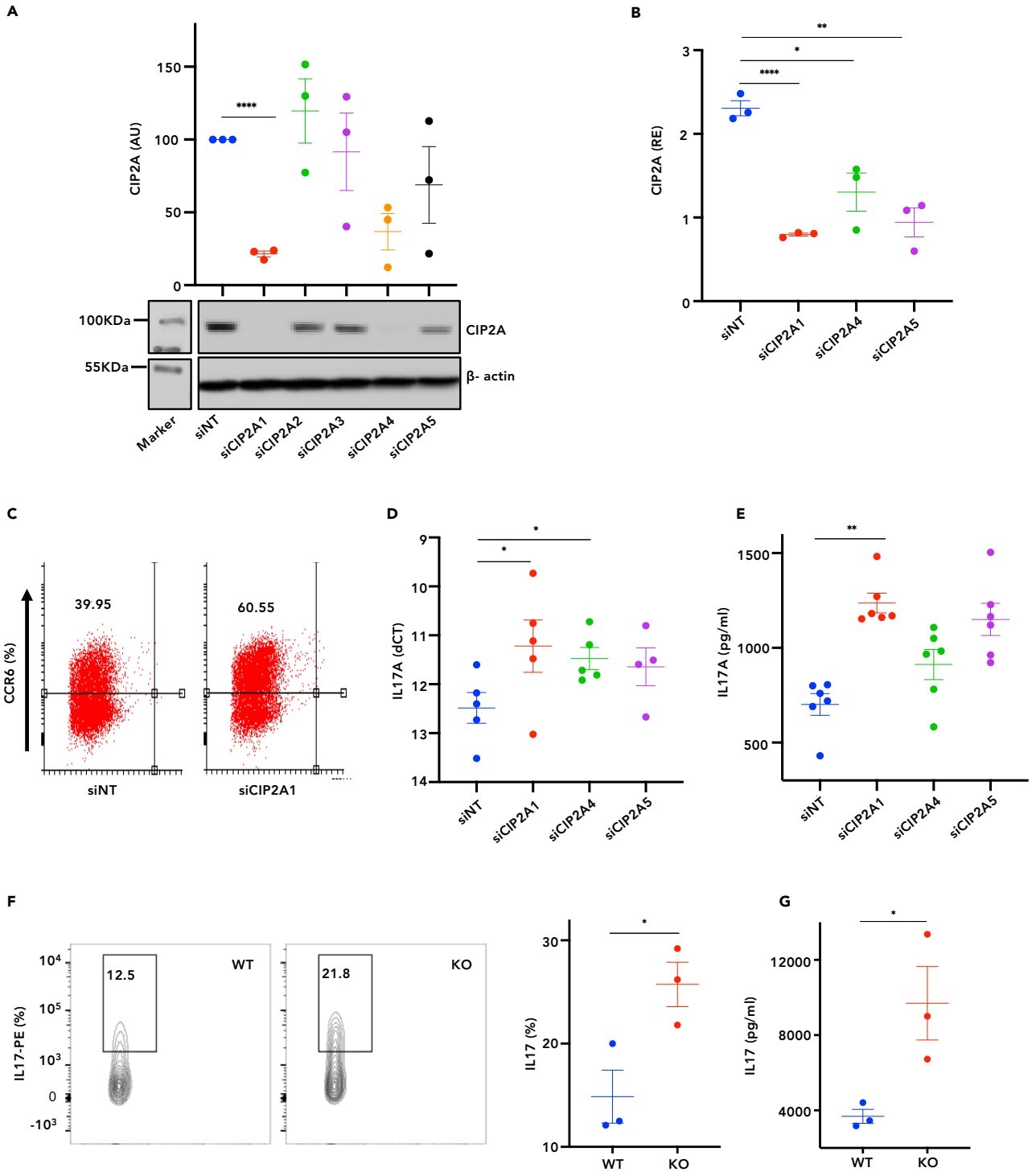

Figure 2. CIP2A Negatively Regulates Th17 Cell Differentiation

(A) Western blot (WB) analysis of CIP2A silencing by five different siRNAs. NT denotes non-targeting siRNA. Quantification was performed using ImageJ software and plotted above the representative WB where each dot represents an independent experiment. The significance was determined using unpaired two-tailed t test; ****$p < 0.0001$.

(B) TaqMan qRT-PCR analysis demonstrating the efficiency of CIP2A silencing by the three functional CIP2A siRNAs shown in (A). The significance was determined using unpaired two-tailed t test; *$p < 0.05$, **$p < 0.01$, ****$p < 0.0001$.

Figure 2. *Continued*

(C) A flow cytometry dot blot analysis of Th17 cell-specific CCR6 receptor expression in CIP2A-silenced and control 72 h polarized human Th17 cells. A representative example of three biological replicates. The number on the plot shows the percentage of positive cells.

(D) TaqMan qRT-PCR analysis of *IL17A* expression in CIP2A-silenced human Th17 cells at 72 h. Asterisks denotes significance obtained in Student's t test (two-tailed paired) with *$p < 0.05$.

(E) Luminex analysis of secreted IL-17A in CIP2A-silenced human Th17 cells. The values were normalized by the number of living cells, determined on the basis of cell size and granularity detected by flow cytometry. The significance obtained by Student's t test (two-tailed paired) with **$p < 0.01$.

(F) Flow cytometry analysis of IL-17A expression in mouse Th17 cells from CIP2A knockout (KO) and control (WT) animals shown as contour plot of one replicate (left) and the mean of three replicates (right). *$p < 0.05$.

(G) Luminex analysis of IL-17A secretion from Th17 cells generated from CIP2A KO and WT mice cells. In TaqMan qRT-PCR analysis unless otherwise stated, data were calculated as dCT values normalized with the housekeeping gene (EF1-alpha) and plotted as 2^{-dCt}. Asterisks denotes significance obtained in Student's t test (two-tailed paired) with *$p < 0.05$.

was true also for mouse, naive CD4+CD62L+ splenic T cells from CIP2A WT and knockout (KO) animals were differentiated to the Th17 direction and IL-17 levels were measured. Similar to human Th17 cells, a consistent increase in IL-17A expression in the CIP2A-deficient mouse Th17 cells was detected at 72 h (Figures 2F and 2G).

To assess whether the increase in IL-17 expression in CIP2A-silenced cells was due to regulation of *IL17A* gene expression, increased proliferation, or increased cell survival, naive CD4+ T cells were labeled with carboxyfluorescein succinimidyl ester (CFSE) and the cells were activated under Th17-promoting conditions. The extent of CFSE dilution was monitored 96 h post cell activation, in both CIP2A-silenced and control cells. The rate of proliferation in CIP2A-silenced cells was slower than in the control cells (Figure S2D). Similar results were also obtained in mouse cells deficient in CIP2A (Figure S2E), and there were no significant differences in the cell viability between the cell populations (Figure S2F). These results confirmed that increase in IL-17 upon CIP2A silencing is not due to increased proliferation of these cells and is consistent with several other reports that have found reduced proliferation of CIP2A-deficient cells in other cell types (Junttila et al., 2007; Ventelä et al., 2012; Yang et al., 2016).

To explore the mechanisms underlying the increased Th17 differentiation of CIP2A-deficient cells, we carried out RNA sequencing (RNA-seq) analysis of CIP2A-silenced cells cultured under Th17 condition for 24 h. This time point was chosen to ensure that CIP2A expression is induced and that the siRNA-mediated silencing of CIP2A remains efficient. CIP2A silencing resulted in differential expression of 136 genes (false discovery rate [FDR] <0.05) in cells differentiated to the Th17 direction for 24 h (Figure 3A and Table S1). Fifty of these genes have been shown to be differentially expressed (DE) during Th17 differentiation (Tuomela et al., 2016) (Table S2). Consistent with the increase in *IL17* expression, many genes encoding Th17-related TFs, e.g., *RORA*, *RORC,* and *MAF,* were upregulated in the CIP2A-deficient Th17 cells. In contrast, several genes that repress Th17 cell differentiation (e.g., interferon-γ, IL-2, and IRF8) were downregulated in CIP2A-deficient conditions suggesting CIP2A negatively regulates Th17 differentiation.

Gene set enrichment analysis (Subramanian et al., 2005) was performed to investigate whether there was a global increase in the expression of Th17 cell signature genes upon CIP2A silencing. The Th17 cell signature genes were defined from our earlier study as the top upregulated (24 h, FDR <0.05, log2[FC] > 2) genes in Th17 conditions (Tuomela et al., 2016). The majority of Th17 cell signature genes were more abundant in the CIP2A-deficient samples than in the control samples (Figure 3B upper panel), indicating a general upregulation of Th17 cell signature genes in CIP2A-deficient Th17 cells. In comparison, the corresponding induced regulatory T cell (iTreg) gene set (24 h, FDR <0.05, log2[FC] > 2) was not enriched (Figure 3B lower panel).

Ingenuity pathway analysis (IPA) of the CIP2A-silenced Th17 cell gene expression data was used to gain an overview of the pathways enriched among the DE genes observed in CIP2A-deficient human Th17 cells and the cellular location of different RNA species among the DE genes. Enzymes were the most enriched class among the DE genes, followed by transporters and transcriptional regulators (Figure 3C). Interestingly, among the most enriched pathways were differential regulation of cytokines by IL-17 in epithelia, macrophages, and Th cells, as well as IL-17 regulation in inflammatory diseases, supporting a role for CIP2A in the regulation of signaling involved in IL-17 expression (Figure 3D).

CIP2A Controls TH17 Differentiation by Regulating STAT3 Phosphorylation

To identify the key upstream regulators of the observed RNA-seq transcriptional signature in CIP2A-deficient Th17 cells, we used "upstream regulators" predictor tool from IPA. The tool predicts the key upstream

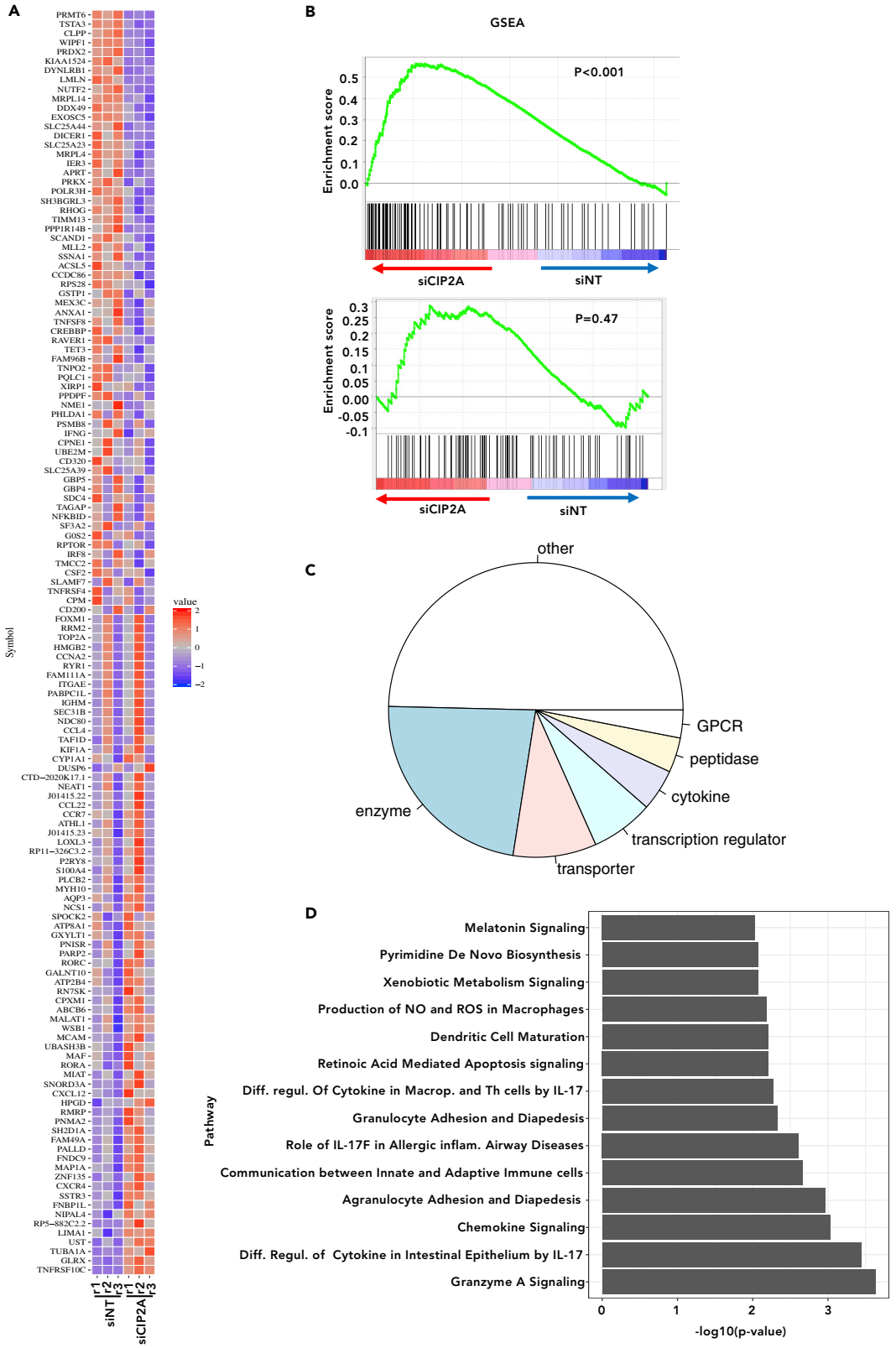
A
Symbol
value
siNT
siCIP2A
B
GSEA
P<0.001
Enrichment score
siCIP2A
siNT
P=0.47
Enrichment score
siCIP2A
siNT
C
other
GPCR
peptidase
cytokine
transcription regulator
transporter
enzyme
D
Pathway
Melatonin Signaling
Pyrimidine De Novo Biosynthesis
Xenobiotic Metabolism Signaling
Production of NO and ROS in Macrophages
Dendritic Cell Maturation
Retinoic Acid Mediated Apoptosis signaling
Diff. regul. Of Cytokine in Macrop. and Th cells by IL-17
Granulocyte Adhesion and Diapedesis
Role of IL-17F in Allergic inflam. Airway Diseases
Communication between Innate and Adaptive Immune cells
Agranulocyte Adhesion and Diapedesis
Chemokine Signaling
Diff. Regul. of Cytokine in Intestinal Epithelium by IL-17
Granzyme A Signaling
-log10(p-value)

Figure 3. Several Genes Are Affected upon CIP2A Silencing in Human Th17 Cells

(A) Genes DE between CIP2A-silenced (siCIP2A1) or control (siNT) Th17 cells (24 h) shown as heatmap. The plot is of *Z* score calculated from RPKM (Reads Per Kilobase of transcript, per Million mapped reads) values. First three columns represent data from siNT, and the last three columns are from siCIP2A-treated cells. "r1," "r2," and "r3" denote three replicates.

(B) Enrichment of Th17 signature genes (24 h log2FC > 2) (Tuomela et al., 2016) is shown in the top panel. Panel on the bottom shows lack of enrichment of iTreg genes. Each vertical line in the plot shows one gene. Lines toward the red indicate genes that are enriched in siCIP2A samples, and those toward the blue indicate enrichment in siNT samples. For details, see Transparent Methods section.

(C) Pie chart showing the distribution of different RNA species among DE genes in the siCIP2A1-treated Th17 cells.

(D) IPA analysis showing enriched pathways among the genes DE in CIP2A-deficient human Th17 cells.

TF or cytokines that may not be upregulated at the RNA level but may have increased activity because of posttranslational modification, e.g., phosphorylation. Interestingly, STAT3, a known positive regulator of Th17 cell differentiation (Chen et al., 2006; Durant et al., 2010; Tripathi et al., 2017), was one of the key upstream regulators predicted to be activated (*Z* score > 2) in CIP2A-deficient cells (Figure 4A). Furthermore, Transcription Factor Binding Sites enrichment analysis on the promoters of DE genes revealed enrichment of several Th17-related factors including STAT3 (Table S3). Based on these results, we hypothesized that enhanced Th17 cell differentiation upon CIP2A deficiency could be due to increased STAT3 activity.

To test whether CIP2A silencing leads to changes in STAT3 activity, levels of STAT3 phosphorylation were determined. Naive CD4+ T cells were activated for 48 h in Th17-polarizing conditions to ensure the expression of CIP2A, and siRNA was then used to silence CIP2A expression. As STAT3 phosphorylation occurs early during Th17 differentiation, cells were re-activated for 15 min under Th17 condition and STAT3 phosphorylation was monitored using intracellular flow cytometry staining and western blotting (WB) (Figure 4B). STAT3 phosphorylation (Y705) was indeed consistently higher in cells depleted of CIP2A by all the three CIP2A siRNAs when compared with controls both in terms of percentage (Figure 4C) and median florescence intensity (Figure 4D). Higher phosphorylation of STAT3 was also observed at serine-727 (Figure S3A). To test whether the increase in pSTAT3 is also sustained for longer duration, we performed similar experiments to those described in Figure 4B, except that the additional time points at 30 and 360 min were included. Interestingly, not only was there an increase in STAT3 phosphorylation but also the phosphorylation was sustained longer in CIP2A-silenced samples (Figure 4E). Besides Tyrosine-705 phosphorylation, serine-727 phosphorylation was also sustained in the CIP2A-deficient Th17 cells (Figure 4E). To test whether the increase in the phosphorylation in CIP2A-deficient cells was specific to STAT3, we measured the phosphorylation of STAT5. As STAT5 is phosphorylated in response to IL-2 stimulation, we first cultured the naive cells as shown in Figure 4B, except that the cells were differentiated under iTreg conditions wherein the cells were activated in the presence of IL-2, all-trans retinoic acid, and transforming growth factor-β. No differences in STAT5 phosphorylation were observed, indicating that the changes were specific to STAT3 (Figures S3B and S3C). Taken together, these results suggest that CIP2A limits Th17 differentiation by modulating STAT3 phosphorylation.

AGK Potentiates STAT3 Phosphorylation in the Absence OF CIP2A

We hypothesized that the increase in pSTAT3 in CIP2A-deficient cells is due to changes in the interacting partners of STAT3 in the presence and the absence of CIP2A. To test this hypothesis, we performed immunoprecipitation (IP) of pSTAT3 (Y705) followed by LC-MS/MS of whole-cell lysates to identify proteins that interact with pSTAT3 in CIP2A-sufficient or CIP2A-deficient conditions in human Th17 cells. Cells were first activated for 48 h under Th17 condition. The cells were then nucleofected, rested, and re-activated for 15 min in Th17-polarizing condition, and pSTAT3 was measured by WB (Figure S3D). STAT3 was enriched many folds in IP samples when compared with control (IgG) samples (Figure 5A). Interestingly, pSTAT3 was higher in siCIP2A when compared with siNT, confirming the results shown in Figures 4C and 4E. Proteins interacting with pSTAT3 were pulled down together with the pSTAT3 and identified by MS analysis. STAT3 was the most enriched protein in MS analysis of both CIP2A-sufficient and CIP2A-deficient conditions, confirming that the IP and MS were successful. Following statistical analysis of the MS data from the IP samples, 335 of the identified proteins were discerned to interact with pSTAT3 in the CIP2A-sufficient or CIP2A-deficient conditions and were distinct from the IgG-only baits (Table S4). The detected interacting proteins were filtered to include those differentially abundant between prey and bait ($p < 0.05$, paired t test) and passing a Significance Analysis of Interactome (SAINT) probability score of >0.7 (Emani et al., 2015). Among these, 217 proteins interacted with pSTAT3 both in CIP2A-sufficient and CIP2A-deficient conditions (Figures 5B and 5C), whereas the interaction of 69 and 49 proteins were distinguished in the CIP2A-sufficient and CIP2A-deficient conditions, respectively (Table S4).

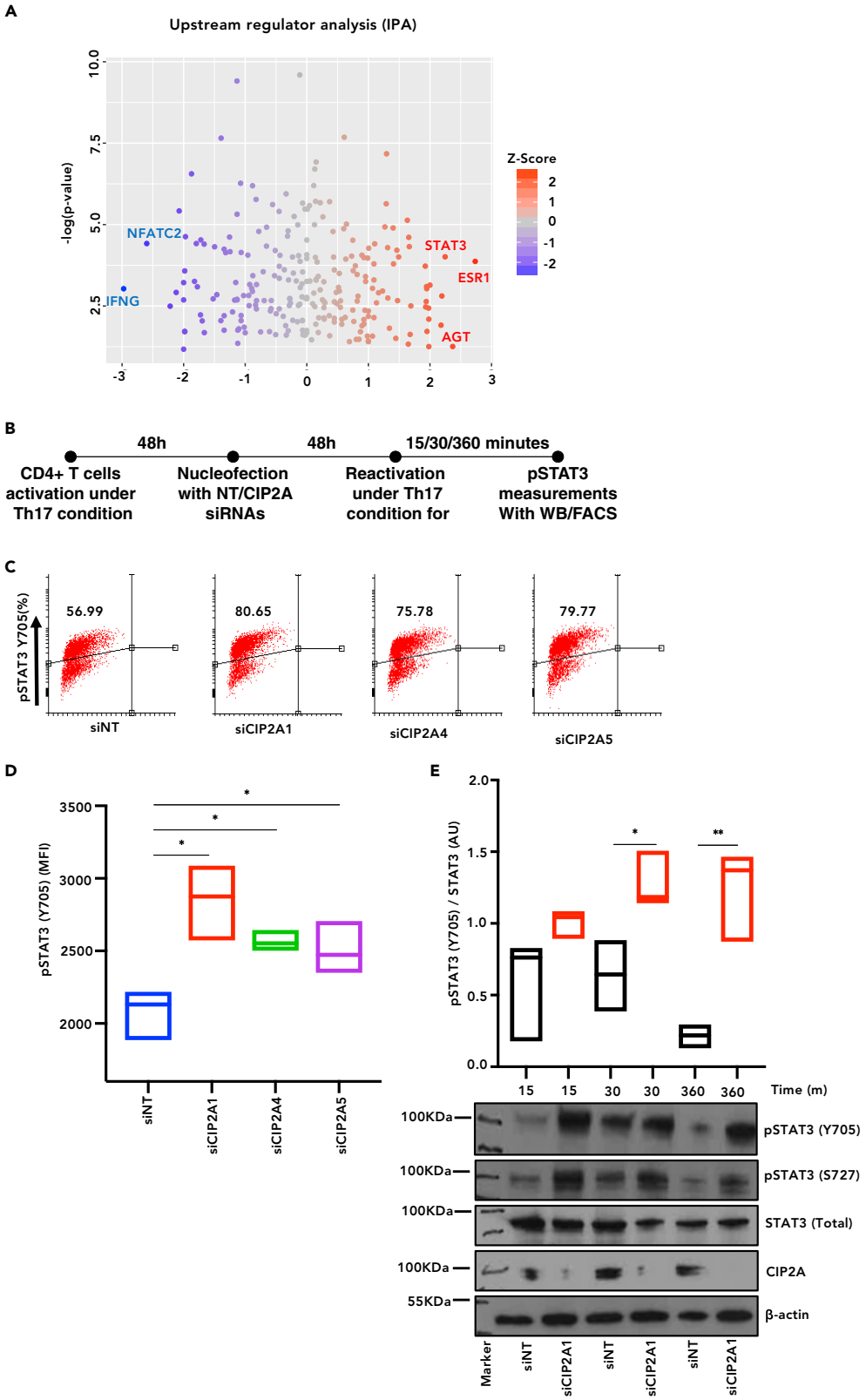
A
Upstream regulator analysis (IPA)
-log(p-value)
10.0
7.5
5.0
2.5
-3
-2
-1
0
1
2
3
NFATC2
IFNG
STAT3
ESR1
AGT
Z-Score
2
1
0
-1
-2
B
48h
48h
15/30/360 minutes
CD4+ T cells activation under Th17 condition
Nucleofection with NT/CIP2A siRNAs
Reactivation under Th17 condition for
pSTAT3 measurements With WB/FACS
C
pSTAT3 Y705(%)
56.99
80.65
75.78
79.77
siNT
siCIP2A1
siCIP2A4
siCIP2A5
D
pSTAT3 (Y705) (MFI)
3500
3000
2500
2000
*
*
*
siNT
siCIP2A1
siCIP2A4
siCIP2A5
E
pSTAT3 (Y705) / STAT3 (AU)
2.0
1.5
1.0
0.5
0.0
*
**
15
15
30
30
360
360
Time (m)
100KDa
pSTAT3 (Y705)
100KDa
pSTAT3 (S727)
100KDa
STAT3 (Total)
100KDa
CIP2A
55KDa
β-actin
Marker
siNT
siCIP2A1
siNT
siCIP2A1
siNT
siCIP2A1

Figure 4. CIP2A Regulates Th17 Differentiation by Modulating STAT3 Phosphorylation

(A) Upstream regulators identified using IPA analysis of human DE genes. *Z* score < −2 or >2 indicate predicted negative and positive upstream regulators, respectively.

(B) Experimental design for studying STAT3 phosphorylation (Y705) in CIP2A-silenced human Th17 cells. Human $CD4^+$ T cells were first activated under Th17 culturing conditions for 48 h. Cells were then harvested and nucleofected with NT or CIP2A siRNA followed by a 48-h rest and then reactivated in the presence of Th17-polarizing cytokines for 15–60 min.

(C) Analysis of STAT3 phosphorylation (Y705) by flow cytometry in cells treated with NT or CIP2A siRNA using culturing conditions as in Figure 4B. Acquisition of the stained cells was made with an LSRII flow cytometer, and data analysis was performed by using either Flowing or FlowJo software (tree star).

(D) Boxplot to represent median fluorescence intensity (MFI) quantification of STAT3 phosphorylation (Y705) in three independent experiments by flow cytometry as shown in Figure 4C.

(E) Analysis of STAT3 phosphorylation (Y705 and S727) by WB. Total STAT3, CIP2A, and beta-actin were detected on the same blot. Quantification was performed using ImageJ software and shown in the form of boxplot for Y705 pSTAT3 above the representative WB. (D and E) Significance obtained in Student's t test (two-tailed unpaired); *$p < 0.05$, **$p < 0.01$.

The STAT3 interactome data were analyzed with Gene Ontology (GO) and network analysis tools to gain an overview of the biological processes associated with the proteins through which STAT3 mediates its function. STAT3-interacting proteins associated with both the CIP2A-sufficient and CIP2A-deficient conditions were selected for the network analysis. A network was constructed using the STRING database (Szklarczyk et al., 2017) to gather the known interactions between the proteins. The resulting network was further visualized with Cytoscape (Shannon et al., 2003) and enriched biological processes were identified using DAVID (Huang et al., 2009a, 2009b) and PANTHER (Mi et al., 2013, 2017), revealing RNA processing, immune response, and cell adhesion as the processes most frequently linked with the STAT3-associated proteins (Figure 5D). Collectively, these results suggest that STAT3 is involved in multiple steps, ranging from RNA production to the production of a functional protein and in cell signaling.

Further analysis of pSTAT3 interactors in IPA revealed enrichment of CD28 signaling in Th cells in CIP2A-sufficient condition (Figures S4A and S4B). Conversely, protein kinase A signaling was enriched among pSTAT3 interactors only under CIP2A-deficient conditions. In terms of their organellar associations, the largest proportion of the pSTAT3 interactors were cytoplasmic, followed by nuclear and plasma membrane, both under CIP2A-sufficient and CIP2A-deficient conditions (Figure S4C). Functionally, the largest proportion of pSTAT3 interactors belonged to "enzymes," followed by transcription regulators and transporters (Figure S4D).

To identify STAT3-interacting partners associated with the increase in pSTAT3 observed in CIP2A-deficient cells, we searched for proteins preferentially interacting with STAT3 either in CIP2A-silenced or control Th17 cells. Interestingly, a significantly enhanced interaction was detected between a lipid kinase AGK and STAT3 in CIP2A-silenced cells (Table S4) when compared with control cells. These results were validated in independent co-IP experiments (Figure 6A). Furthermore, using confocal microscopy, we detected a significantly higher co-localization of AGK and pSTAT3 in CIP2A-deficient human Th17 cells than in control cells (Figure 6B). Notably, AGK was also identified as a CIP2A-interacting protein in a reciprocal CIP2A IP experiment (Figure 6C left). The CIP2A-AGK interaction was further confirmed by targeted selected reaction monitoring-based MS analysis of CIP2A IP samples (Figure 6C right). It has been reported that AGK directly interacts with STAT3 in cancer cells and promotes its phosphorylation by JAKs (Chen et al., 2013). Silencing of AGK decreased pSTAT3 (Y705) levels, whereas its overexpression led to an increase in pSTAT3 (Y705) levels (Chen et al., 2013). We confirmed that indeed AGK-pSTAT3 interaction is enhanced in the absence of CIP2A. We tested if AGK silencing will bring back the increased phosphorylation of STAT3 in CIP2A-deficient Th17 cells. First, we efficiently silenced AGK using three different siRNAs (Figure 6D). STAT3 levels were unaffected, as reported earlier in epithelial cells (Chen et al., 2013), whereas AGK silencing significantly reduced pSTAT3 in Th17 cells (Figure 6D). Furthermore, depletion of AGK in CIP2A-silenced cells was able to neutralize the enhanced pSTAT3 levels as measured both by flow cytometry (Figures 6E and 6F) and WB analysis (Figure 6G), as well as enhanced IL-17 production (Figure 6H). Taken together these data suggest that CIP2A interacts with AGK, regulates the interaction between AGK and STAT3, and thereby controls the phosphorylation of STAT3 in Th17 cells.

Regulation of TH17 Differentiation by CIP2A and by Inhibition of PP2A Catalytic Phosphatase Activity

In mouse T cells, overexpression of PP2A catalytic subunit (PP2Ac) was shown to facilitate the transcription of pro-inflammatory genes including *IL17A* (Apostolidis et al., 2013). In addition, PP2Ac was recently

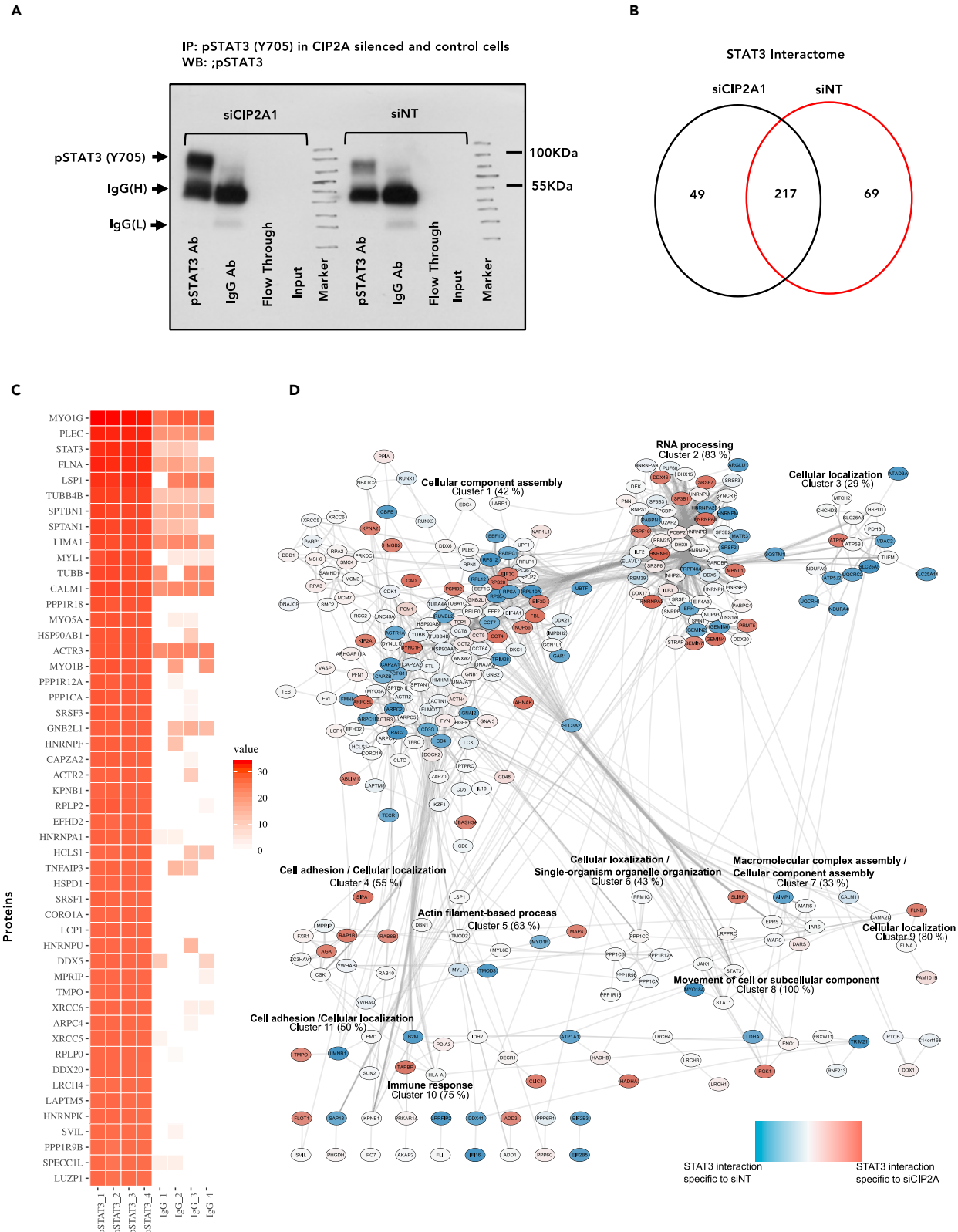
A
IP: pSTAT3 (Y705) in CIP2A silenced and control cells
WB: ;pSTAT3
siCIP2A1
siNT
pSTAT3 (Y705)
IgG(H)
IgG(L)
100KDa
55KDa
pSTAT3 Ab
IgG Ab
Flow Through
Input
Marker
B
STAT3 Interactome
siCIP2A1
siNT
49
217
69
C
Proteins
value
30
20
10
0
pSTAT3_1
pSTAT3_2
pSTAT3_3
pSTAT3_4
IgG_1
IgG_2
IgG_3
IgG_4
D
RNA processing
Cluster 2 (83 %)
Cellular component assembly
Cluster 1 (42 %)
Cellular localization
Cluster 3 (29 %)
Cell adhesion / Cellular localization
Cluster 4 (55 %)
Cellular loxalization /
Single-organism organelle organization
Cluster 6 (43 %)
Macromolecular complex assembly /
Cellular component assembly
Cluster 7 (33 %)
Actin filament-based process
Cluster 5 (63 %)
Cellular localization
Cluster 9 (80 %)
Movement of cell or subcellular component
Cluster 8 (100 %)
Cell adhesion /Cellular localization
Cluster 11 (50 %)
Immune response
Cluster 10 (75 %)
STAT3 interaction
specific to siNT
STAT3 interaction
specific to siCIP2A

Figure 5. Phospho-STAT3 (Y705) Interactome in CIP2A-Silenced Human Th17 Cells

(A) Western blot (WB) analysis of pSTAT3 (Y705) immunoprecipitation (IP) in CIP2A-silenced and control Th17 cells (cultured as indicated in Figure 4B). Representative IP WB, input, flow-through (FT), IgG control IP, and pSTAT3 IP lanes are shown.

(B) A Venn diagram of the proteins interacting with pSTAT3 (Y705) under CIP2A-deficient (siCIP2A) or CIP2A-sufficient (siNT) Th17 cells.

(C) Heatmap showing top 50 proteins interacting with pSTAT3 (Y705) in control and CIP2A-silenced Th17 cells in four replicate experiments. Log2-transformed intensity values are plotted.

(D) Network STAT3-interacting proteins generated using STRING database and visualized using the Cytoscape software. The nodes in the network were clustered using the Markov clustering algorithm. The most enriched GO biological process term is shown for each cluster with four or more members. The strength of interaction with STAT3 in the different conditions is indicated by the coloring of the nodes. Blue color corresponds to interactions with STAT3 only in the siNT condition, red color indicates interactions with STAT3 only in the siCIP2A condition, and white corresponds to interactions of equal strength in both conditions.

identified as an essential regulator of Th17 differentiation. T cell-specific deletion of PP2Ac (*Ppp2ca*) resulted in impaired Th17 differentiation and rendered mice resistance to myelin oligodendrocyte glycoprotein-induced experimental autoimmune encephalomyelitis (Xu et al., 2019). Thereby, the results that both CIP2A and PP2A inhibit IL-17 expression in humans could be reconciled by the current model that CIP2A does not regulate catalytic PP2Ac subunit phosphatase activity, but more selectively modulates PP2A/B56 complex substrate recognition (Junttila et al., 2007; Wang et al., 2017).

To further study this, we directly compared the role of CIP2A and PP2Ac catalytic activity in regulation of IL-17 gene expression. First, we silenced the PP2A-A subunit, which is a scaffold for PP2A complex and essential for PP2A activity, using two different concentrations of the siRNA-targeting PP2A-A subunit (Figures 7A and S5A). PP2A-A silencing led to a significant increase in IL-17 expression both at RNA (Figure 7B) and protein (Figure 7C) levels. Furthermore, we modulated the activity of PP2A either by a chemical inhibitor or activator, and measured IL-17 expression at RNA and protein levels. Serine/threonine phosphatase inhibitor okadaic acid (OA) was used to inhibit PP2A in Th17 cells. The applied concentration of 10 nM was selected to achieve relative selectivity toward PP2A over PP1, PP4, and PP6 (Apostolidis et al., 2013). This concentration was well tolerated by T cells (Figure S5B). Similar to siRNA-mediated inhibition of PP2A-A, treatment of cells with OA led to increased production of IL-17 (Figures 7D and 7E). Furthermore, treatment with FTY720 (2-amino-2-[2-(4-octylphenyl) ethyl] propane-1,3-diol; Fingolimod, Novartis), which directly activates PP2Ac via blocking binding of PP2A inhibitor (I2PP2A/SET) (Saddoughi et al., 2013; Switzer et al., 2011), led to reduced IL-17 levels (Figures 7F and 7G). Together, these results demonstrate opposite outcomes by direct modulation of PP2Ac catalytic activity or by B56-selective modulation of PP2A via CIP2A. This in turn provides a unique opportunity for immunomodulation, which cannot be predicted from the effects induced by direct manipulation of PP2A catalytic activity toward presumably all PP2A-regulated targets.

DISCUSSION

CIP2A is upregulated in a variety of human cancers. Its inhibitory function toward PP2A/B56 thereby stabilizes the oncoprotein MYC in cancer cells (Junttila et al., 2007; Khanna et al., 2013; De et al., 2014). Here, we delineate previously unappreciated immune regulatory role of CIP2A and demonstrate that it acts as a negative regulator of human and mouse Th17 cell differentiation. Our data revealed that CIP2A silencing results in increased expression of proinflammatory cytokine IL-17 at both the protein and RNA levels. Consistent with increased IL17 in CIP2A-deficient cells, IRF8, a negative regulator of Th17 cell differentiation (Ouyang et al., 2011), was downregulated upon CIP2A silencing (Figure 3A). Furthermore, several Th17-related TFs were upregulated including RORC, RORA, and MAF (Figure 3A).

Moreover, CIP2A deficiency led to enhanced expression of factors important for Th17 differentiation, including phosphorylation of STAT3. Altered signaling of STATs or their negative regulators can lead to pathological conditions such as chronic inflammation, inadequate immune response, or cancer (Grivennikov et al., 2010; Multhoff et al., 2011; Landskron et al., 2014). Enhanced STAT3 phosphorylation in CIP2A-silenced human Th17 cells may explain upregulation of Th17-related genes in human and mouse CIP2A-deficient Th17 cells. STAT3 is a key upstream factor driving Th17 differentiation. It also plays an important role in many other types of cells including cancer cells. In spite of these, STAT3 interactome has not been studied previously in Th17 cells. In this study, we delineated pSTAT3 interactome in CIP2A-silenced and control cells. Our data revealed many new protein interactions with STAT3 including ubiquitin ligase TRIM21 and kinase AGK. The interactome of pSTAT3 identified in this study can be used as a resource for future studies aiming at further understanding of STAT3 functions.

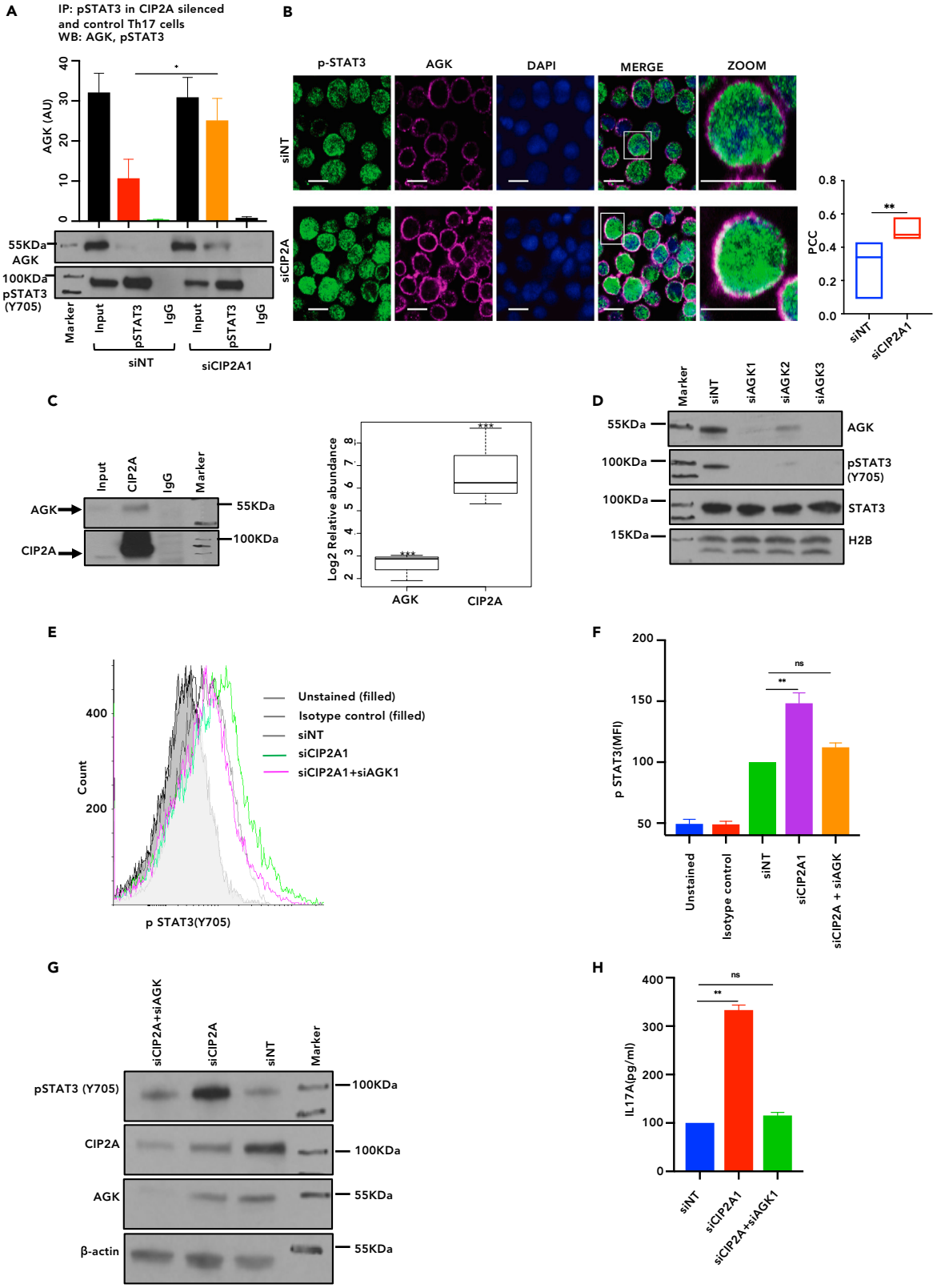
A
IP: pSTAT3 in CIP2A silenced and control Th17 cells
WB: AGK, pSTAT3
AGK (AU)
55KDa AGK
100KDa pSTAT3 (Y705)
Marker
Input
pSTAT3
IgG
siNT
siCIP2A1
B
p-STAT3
AGK
DAPI
MERGE
ZOOM
siNT
siCIP2A
PCC
C
Input
CIP2A
IgG
Marker
AGK
CIP2A
55KDa
100KDa
Log2 Relative abundance
D
Marker
siNT
siAGK1
siAGK2
siAGK3
55KDa
100KDa
15KDa
AGK
pSTAT3 (Y705)
STAT3
H2B
E
Unstained (filled)
Isotype control (filled)
siNT
siCIP2A1
siCIP2A1+siAGK1
Count
p STAT3(Y705)
F
p STAT3(MFI)
Unstained
Isotype control
siNT
siCIP2A1
siCIP2A + siAGK
G
siCIP2A+siAGK
siCIP2A
siNT
Marker
pSTAT3 (Y705)
CIP2A
AGK
β-actin
100KDa
55KDa
H
IL17A(pg/ml)
siNT
siCIP2A1
siCIP2A+siAGK1

Figure 6. AGK Potentiates STAT3 Phosphorylation in the Absence of CIP2A

(A) pSTAT3 IP experiment showing its interaction with AGK in CIP2A-silenced and control Th17 cells. Quantification performed by ImageJ and shown in the form of bar graph of the WB from four replicate experiments. Statistics by Student's t test, two-tailed paired, *$p < 0.05$. Error bars represent SEM in the figure.

(B) Representative confocal images of three replicates for studying co-localization of pSTAT3 (Y705) and AGK in CIP2A-silenced (lower panel) and control (upper panel) Th17 cells by Zeiss LSM780 confocal microscope. Cells were stained for endogenous pSTAT3 (green), AGK (magenta), and nuclei (DAPI). Scale bar, 7 μm. Pearson's correlation coefficient (PCC) for data on the right plotted as boxplot and determined by ImageJ software cloloc2 plugin ($n > 30$ cells). Statistics by Student's t test, two-tailed paired, **$p < 0.01$.

(C) The left panel shows the WB analysis of co-IP of AGK and CIP2A by anti-CIP2A pull-down in human Th17 cells 72 h post cell activation. In the representative blot of two experiments, input, IgG control IP, and CIP2A IP lanes are shown. The right panel shows selected reaction monitoring targeted mass spectrometry showing interaction of AGK and CIP2A in 72 h polarized Th17. Averaged results from three replicates are presented in the form of a boxplot. Statistical significance was determined using a two-tailed paired Student's t test; ***$p < 0.001$. The error bars represent 95% confidence interval.

(D) Representative WB of two replicates showing AGK silencing by three individual AGK siRNAs. The effect of siRNA-mediated AGK depletion on pSTAT3 (Y705) expression in 15-min reactivated Th17 cells, prepared as described in Figure 4B, is also shown. Histone 2B was used as a loading control.

(E and F) Flow cytometry analysis of pSTAT3 in control, CIP2A-silenced, and CIP2A/AGK double-silenced human Th17 cells shown as overlapping histograms (E) and bar charts of MFI from four biological replicates (F). Statistics by a two-tailed paired Student's t test, **$p < 0.01$. The error bars represent SEM in the figure.

(G) A representative WB analysis of four experiments showing expression of pSTAT3 (Y705) in Th17 cells treated with siNT, siCIP2A, or siCIP2A + siAGK siRNAs. Cells were cultured and nucleofected as described in Figure 4B.

(H) Secretion of IL-17A (pg/mL) measured by Luminex at 72 h following cell activation in Th17 cells treated with siNT, siCIP2A, or siCIP2A + siAGK siRNAs. Statistics by a two-tailed paired Student's t test, **$p < 0.01$. The error bars represent SEM in the figure.

AGK preferentially interacts with pSTAT3 in CIP2A-deficient cells. In cancer cells, AGK facilitates STAT3 phosphorylation by inhibiting autoinhibitory JH2 domain on JAK2 to phosphorylate STAT3 (Chen et al., 2013). Similar to cancer cells, AGK silencing resulted in reduced STAT3 phosphorylation in Th17 cells. We demonstrated that in CIP2A-silenced cells, increased interaction between AGK and STAT3 results in enhanced pSTAT3. Thus, we propose that CIP2A regulates the strength and duration of STAT3 phosphorylation in Th17 cells by regulating AGK-STAT3 interaction in Th17 cells.

TRIM21 deficiency in mice leads to enhanced production of the pro-inflammatory cytokines, IL-6, IL-12, IL-23, and IL-17 (Espinosa et al., 2009) as well as tissue inflammation and systemic autoimmunity through the IL-23-Th17 pathway (Espinosa et al., 2009; Chikuma et al., 2012; Ahn et al., 2017). Interestingly, TRIM21 interacts with IRF8 (Yang et al., 2009; Yoshimi et al., 2012; Lazzari et al., 2014), a negative regulator of Th17 differentiation (Ouyang et al., 2011) and marks it for degradation by proteasomes (Yang et al., 2009; Yoshimi et al., 2012; Lazzari et al., 2014). Further studies are required to clarify if the reduced interaction between STAT3 and TRIM21, as well as reduced IRF8 expression in CIP2A-silenced human Th17 cells, contributes to enhanced Th17 differentiation.

CIP2A was initially identified as a PP2A-interacting protein (Junttila et al., 2007). In agreement with this, in a parallel study, we found CIP2A to interact with PP2A subunits in Th17 cells (Khan et al., 2020). Previously, it was shown that overexpression of PP2A catalytic subunit in mice led to increased IL-17 production (Apostolidis et al., 2013). Recently, impaired Th17 differentiation was demonstrated in mice with PP2A catalytic subunit gene (Ppp2ca) KO specific to T cells (Xu et al., 2019). Contrary to the findings in mouse, we observed increased IL-17 production upon PP2A inhibition by siRNA and OA. Furthermore, treatment with PP2A activator FTY720 led to reduced IL-17 levels in human Th17 cells. Interestingly, FTY720 has also been used as an immunosuppressant drug for the treatment of patients with multiple sclerosis. Oral treatment with FTY720 reduced the number of IL-17-producing Th17 cells in peripheral blood when compared with placebo-treated patients (Mehling et al., 2008; Brinkmann, 2009; Chun and Hartung, 2010). Thus, the effect of PP2A inhibition on Th17 cells appears to be opposite in human and mouse. Other species-specific examples of gene function are known in the literature, such as SATB1. SATB1-deficient human T cells upon Th17 differentiation produced increased IL-17 (Tripathi et al., 2019), whereas in mouse, SATB1 deficiency led to reduced IL-17 levels (Ciofani et al., 2012). In addition, both inhibition of total catalytic activity of PP2A and inhibition of CIP2A resulted in IL-17 induction, highlighting the substrate selectivity of CIP2A toward PP2A/B56 (Wang et al., 2017). Thus, these results emphasize the significance of PP2A-mediated responses in human Th17 cells.

Using mouse cells, in this study we show that the function of CIP2A in Th17 regulation is conserved in mice and the effect on Th17 differentiation is more pronounced when the knockdown of CIP2A is more efficient. Nevertheless, we focused on human cells because the details of CIP2A function in human and mouse system may not be similar. Furthermore, the *in vivo* results in mouse regarding regulation of Th17

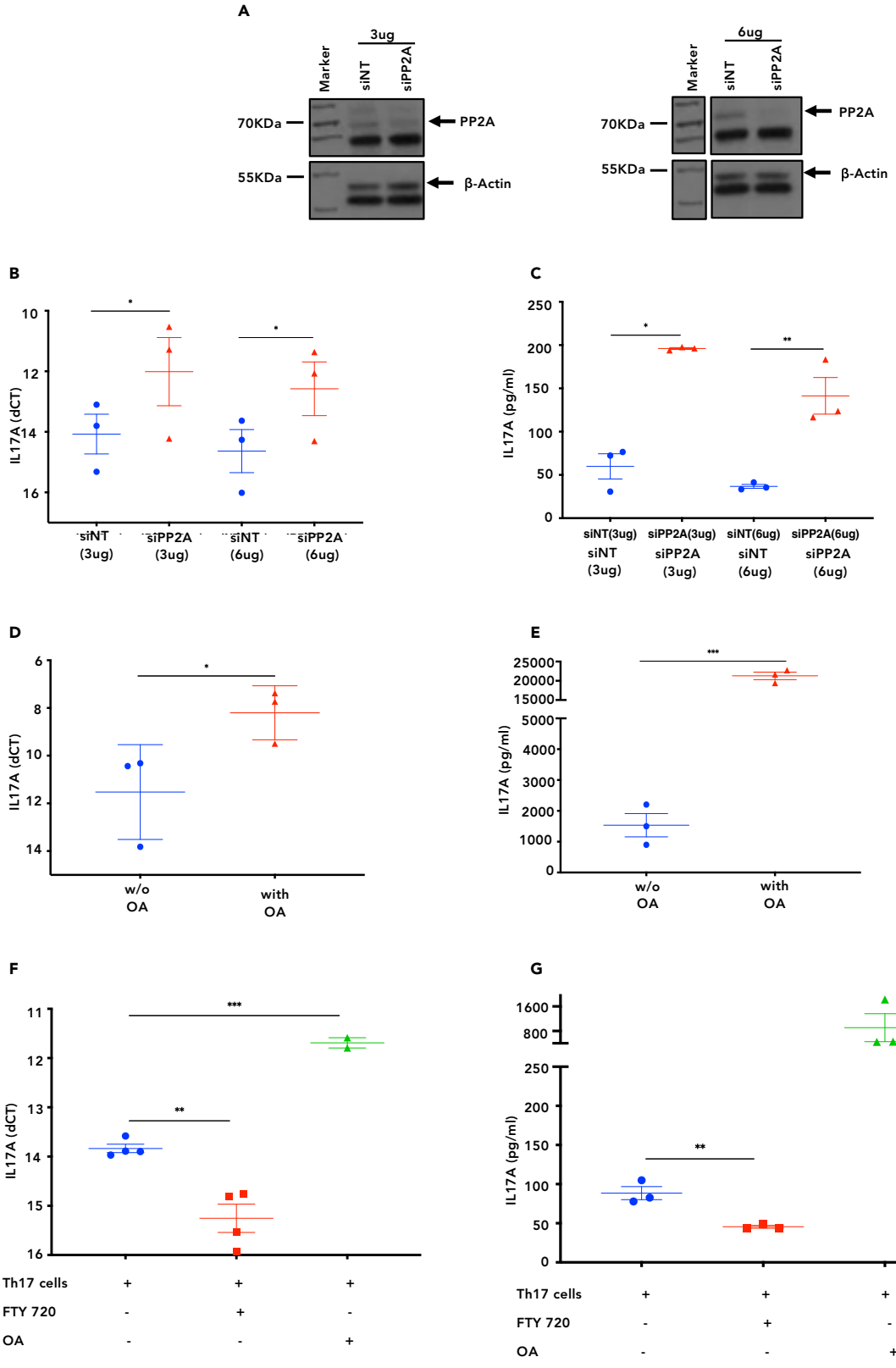
A
3ug
Marker
siNT
siPP2A
70KDa
PP2A
55KDa
β-Actin
6ug
Marker
siNT
siPP2A
70KDa
PP2A
55KDa
β-Actin
B
IL17A (dCT)
siNT (3ug)
siPP2A (3ug)
siNT (6ug)
siPP2A (6ug)
C
IL17A (pg/ml)
siNT(3ug) siNT (3ug)
siPP2A(3ug) siPP2A (3ug)
siNT(6ug) siNT (6ug)
siPP2A(6ug) siPP2A (6ug)
D
IL17A (dCT)
w/o OA
with OA
E
IL17A (pg/ml)
w/o OA
with OA
F
IL17A (dCT)
Th17 cells + + +
FTY 720 - + -
OA - - +
G
IL17A (pg/ml)
Th17 cells + + +
FTY 720 - + -
OA - - +

Figure 7. PP2A Inhibition Enhances IL-17A Production in Human Th17 Cells

(A) Representative WB analysis of PP2A-silenced Th17 cells. Two different concentrations (3 and 6 μg) of PP2A siRNA were used to deplete PP2A in human Th17 cells. Beta-actin was used as loading control.

(B and C) TaqMan PCR analysis of IL-17A expression (B) and Luminex detection of IL-17A protein secretion (C) in PP2A-silenced Th17 cells where each point represents individual replicate. PP2A was silenced as described in (A). Protein measurements of the Luminex analysis was normalized with the sample cell number detected with flow cytometry. Expression at RNA level (dCt) was measured relative to EF1-alpha. Statistics by a two-tailed paired Student's t test; *$p < 0.05$, **$p < 0.01$.

(D and E) PP2A inhibition by okadiac acid (OA) followed by TaqMan PCR analysis of IL-17A expression (D) or Luminex analysis for measuring IL-17 secretion from culture supernatant from three replicate experiments (E). OA was added at the start of the culture. Statistics by a two-tailed paired Student's t test; *$p < 0.05$, ***$p < 0.001$.

(F and G) PP2A activation for 72 h in cells polarizing toward Th17 by FTY 720 in three replicates. IL-17A mRNA expression and IL-17A protein secretion were detected by TaqMan PCR (F) and Luminex (G) analysis, respectively. In TaqMan PCR analysis, dCT was calculated relative to EF1-alpha, and in Luminex, OA was used as a control. Statistics by a two-tailed unpaired Student's t test; **$p < 0.01$, ***$p < 0.001$.

differentiation by PP2A suggest exactly the opposite of what we found in human cells. Thus, a better understanding of the regulation of Th17 cells by CIP2A may provide new approaches for therapeutic intervention in autoimmune and inflammatory diseases as well as in cancer. Overall, our results indicate that CIP2A expression influences several mechanisms important for Th17 response and associated regulation of the immune system that could provide useful insight for the use of CIP2A targeting in cancer therapy.

LIMITATIONS OF THE STUDY

One of the limitations of the study is the lack of *in vivo* data. It remains to be seen if the increase in IL17 expression upon CIP2A silencing leads to the increased propensity of IL-17-mediated inflammatory disease. However, there is a growing consensus that human and mouse systems are different at multiple levels. Indeed, we showed earlier that there is only a little overlap between human and mouse Th17 cell differentiation (Tuomela et al., 2016; Tripathi et al., 2019). Therefore, caution is required in interpreting the results from mouse versus human as fundamental regulatory differences may exist between the two species. Another limitation of the study is that the mechanism of AGK action on STAT3 phosphorylation was not completely delineated. As pointed out earlier in the discussion, in cancer cells, it was demonstrated that AGK removes an autoinhibitory domain of JAK2 to facilitate STAT3 phosphorylation (Chen et al., 2013). We showed that (1) AGK interacts with STAT3, (2) silencing of AGK results in reduced STAT3 phosphorylation, (3) AGK interacts with pSTAT3, and (4) STAT3 phosphorylation is reduced in AGK-depleted Th17 cells suggesting that a similar mechanism operates in Th17 cells. However, further experiments are needed to address the detailed mechanism.

ETHICAL APPROVAL

Ethics Committee of Hospital District of Southwest Finland approved usage of the blood of unknown donors. The animal cells were used according to the university animal welfare guidelines.

METHODS

All methods can be found in the accompanying Transparent Methods supplemental file.

DATA AND CODE AVAILABILITY

The accession number for the RNA-seq data shown in this paper is GSE118094. The mass spectrometry proteomics data have been deposited to the ProteomeXchange Consortium via the PRIDE (Vizcaíno et al., 2016) partner repository with the dataset identifier PXD010612.

SUPPLEMENTAL INFORMATION

Supplemental Information can be found online at https://doi.org/10.1016/j.isci.2020.100947.

ACKNOWLEDGMENTS

We thank the staff of Turku University Hospital, Department of Obstetrics and Gynecology, Maternity Ward, for the cord blood collection. We also thank Marjo Hakkarainen and Sarita Heinonen for excellent technical help. We also duly acknowledge core facilities at the department, namely, the Finnish Functional Genomics Centre (FFGC), the Proteomics Facility, and Cell Imaging Core (CIC) Facility supported by BioCenter Finland. The Finnish Centre for Scientific Computing (CSC) is duly acknowledged for their efficient

servers and their resources in data analysis. M.M.K. was supported by University of Turku graduate school on Turku Doctoral Programme of Molecular Medicine (TuDMM) as well as a central grant from Finnish Cultural Foundation. R.L. was supported by the Academy of Finland, AoF, Centre of Excellence in Molecular Systems Immunology and Physiology Research (2012-2017) grant 250114; by the AoF grants 292335, 294337, 292482, and 31444; by grants from the JDRF; the Sigrid Jusélius Foundation; and the Finnish Cancer Foundation. Z.C. was funded by Academy of Finland grant no. 258313, and J.W. was funded by Sigrid Jusélius Foundation.

AUTHOR CONTRIBUTIONS

M.M.K. designed and performed the experiments, analyzed data, prepared figures, and wrote the manuscript; U.U. designed experiments, analyzed data, prepared figures, and wrote the manuscript; M.H.K. designed and performed the experiments, analyzed data, and prepared figures; L.K. analyzed and prepared figures for RNA-seq data; T.V. performed network and enrichment analysis of STAT interactome and wrote related legends and methods in manuscript; R.M. analyzed the proteomics data and contributed to writing the manuscript; S.D.B. performed the proteomics experiments data analysis; E.K. performed experiments; O.R. designed the experiments, analyzed the data, and wrote the manuscript; Z.C. designed experiments and provided scientific input, expertise, and feedback on the manuscript; L.L.E. supervised T.V. and provided scientific expertise and feedback on the manuscript; J.W. provided scientific input, expertise, mice, and reagents and edited the manuscript; R.L. designed and supervised the study and wrote the manuscript.

DECLARATION OF INTERESTS

The authors declare no competing interests.

Received: December 26, 2019
Revised: February 10, 2020
Accepted: February 21, 2020
Published: March 27, 2020

REFERENCES

Ahn, Y., Hwang, J.H., Zheng, Z., Bang, D., and Kim, D.Y. (2017). Enhancement of Th1/Th17 inflammation by TRIM21 in Behçet's disease. Sci. Rep. *7*, 3018.

Apostolidis, S.A., Rauen, T., Hedrich, C.M., Tsokos, G.C., and Crispín, J.C. (2013). Protein phosphatase 2A enables expression of interleukin 17 (IL-17) through chromatin remodeling. J. Biol. Chem. *288*, 26775–26784.

Brinkmann, V. (2009). FTY720 (fingolimod) in Multiple Sclerosis: therapeutic effects in the immune and the central nervous system. Br. J. Pharmacol. *158*, 1173.

Chen, Z., Laurence, A., Kanno, Y., Pacher-Zavisin, M., Zhu, B.M., Tato, C., Yoshimura, A., Hennighausen, L., and O'Shea, J.J. (2006). Selective regulatory function of Socs3 in the formation of IL-17-secreting T cells. Proc. Natl. Acad. Sci. U S A *103*, 8137–8142.

Chen, X., Ying, Z., Lin, X., Lin, H., Wu, J., Li, M., and Song, L. (2013). Acylglycerol kinase augments JAK2/STAT3 signaling in esophageal squamous cells. J. Clin. Invest. *123*, 2576–2589.

Chikuma, S., Suita, N., Okazaki, I.M., Shibayama, S., and Honjo, T. (2012). TRIM28 prevents autoinflammatory T cell development in vivo. Nat. Immunol. *13*, 596–603.

Chun, J., and Hartung, H.-P. (2010). Mechanism of action of oral fingolimod (FTY720) in multiple sclerosis. Clin. Neuropharmacol. *33*, 91–101.

Ciofani, M., Madar A, Galan C., Sellars, M., Mace, K., Pauli, F., Agarwal, A., Huang, W., Parkhurst, C.N., Muratet, M., Newberry, K.M., et al. (2012). A validated regulatory network for Th17 cell specification. Cell *151*, 289–303.

Côme, C., Cvrljevic, A., Khan, M.M., Treise, I., Adler, T., Aguilar-Pimentel, J.A., Au-Yeung, B., Sittig, E., Laajala, T.D., Chen, Y., et al. (2016). CIP2A promotes T-cell activation and immune response to Listeria monocytogenes infection. PLoS One *11*, 1–18.

De, P., Carlson, J., Leyland-Jones, B., and Dey, N. (2014). Oncogenic nexus of cancerous inhibitor of protein phosphatase 2A (CIP2A): an oncoprotein with many hands. Oncotarget *5*, 4581–4602.

Durant, L., Watford, W.T., Ramos, H.L., Laurence, A., Vahedi, G., Wei, L., Takahashi, H., Sun, H.W., Kanno, Y., Powrie, F., and O'Shea, J.J. (2010). Diverse targets of the transcription factor STAT3 contribute to T cell pathogenicity and homeostasis. Immunity *32*, 605–615.

Emani, M.R., Närvä, E., Stubb, A., Chakroborty, D., Viitala, M., Rokka, A., Rahkonen, N., Moulder, R., Denessiouk, K., Trokovic, R., et al. (2015). The L1TD1 protein interactome reveals the importance of post-transcriptional regulation in human pluripotency. Stem Cell Rep. *4*, 519–528.

Espinosa, A., Dardalhon, V., Brauner, S., Ambrosi, A., Higgs, R., Quintana, F.J., Sjöstrand, M., Eloranta, M.L., Ní Gabhann, J., Winqvist, O., et al. (2009). Loss of the lupus autoantigen Ro52/Trim21 induces tissue inflammation and systemic autoimmunity by disregulating the IL-23–Th17 pathway. J. Exp. Med. *206*, 1661–1671.

Gaffen, S.L., Hernández-Santos, N., and Peterson, A.C. (2011). IL-17 signaling in host defense against Candida albicans. Immunol. Res. *50*, 181–187.

Grivennikov, S.I., Greten, F.R., and Karin, M. (2010). Immunity, inflammation, and cancer. Cell *140*, 883–899.

Huang, D.W., Sherman, B.T., and Lempicki, R.A. (2009a). Bioinformatics enrichment tools: paths toward the comprehensive functional analysis of large gene lists. Nucleic Acids Res. *37*, 1–13.

Huang, D.W., Sherman, B.T., and Lempicki, R.A. (2009b). Systematic and integrative analysis of large gene lists using DAVID bioinformatics resources. Nat. Protoc. *4*, 44–57.

Huh, J.R., Leung, M.W., Huang, P., Ryan, D.A., Krout, M.R., Malapaka, R.R., Chow, J., Manel, N., Ciofani, M., Kim, S.V., et al. (2011). Digoxin and its derivatives suppress TH17 cell differentiation by antagonizing RORγt activity. Nature *472*, 486–490.

Janghorban, M., Farrell, A.S., Allen-Petersen, B.L., Pelz, C., Daniel, C.J., Oddo, J., Langer, E.M., Christensen, D.J., and Sears, R.C. (2014). Targeting c-MYC by antagonizing PP2A inhibitors in breast cancer. Proc. Natl. Acad. Sci. U S A *111*, 9157–9162.

Junttila, M.R., Puustinen, P., Niemelä, M., Ahola, R., Arnold, H., Böttzauw, T., Ala-aho, R., Nielsen, C., Ivaska, J., Taya, Y., et al. (2007). CIP2A inhibits PP2A in human malignancies. Cell *130*, 51–62.

Kanduri, K., Tripathi, S., Larjo, A., Mannerström, H., Ullah, U., Lund, R., Hawkins, R.D., Ren, B., Lähdesmäki, H., and Lahesmaa, R. (2015). Identification of global regulators of T-helper cell lineage specification. Genome Med. *7*, 122.

Kauko, O., and Westermarck, J. (2018). Non-genomic mechanisms of protein phosphatase 2A (PP2A) regulation in cancer. Int. J. Biochem. Cell Biol. *96*, 157–164.

Khan, M.M., Välikangas, T., Khan, M.H., Moulder, R., Ullah, U., Bhosale, S.D., Komsi, E., Butt, U., Westermarck, J., Elo, L.L., and Lahesmaa, R. (2020). Protein interactome of the cancerous inhibitor of protein phosphatase 2A (CIP2A) in Th17 cells. Curr. Res. Immunol. https://doi.org/10.1016/j.crimmu.2020.02.001.

Khanna, A., Pimanda, J.E., and Westermarck, J. (2013). Cancerous inhibitor of protein phosphatase 2a, an emerging human oncoprotein and a potential cancer therapy target. Cancer Res. *73*, 6548–6553.

Kleinewietfeld, M., and Hafler, D.A. (2013). The plasticity of human Treg and Th17 cells and its role in autoimmunity. Semin. Immunol. *25*, 305–312.

Kleinewietfeld, M., Manzel, A., Titze, J., Kvakan, H., Yosef, N., Linker, R.A., Muller, D.N., and Hafler, D.A. (2013). Sodium chloride drives autoimmune disease by the induction of pathogenic TH17 cells. Nature *496*, 518–522.

Landskron, G., De la Fuente, M., Thuwajit, P., Thuwajit, C., and Hermoso, M.A. (2014). Chronic inflammation and cytokines in the tumor microenvironment. J. Immunol. Res. *2014*, 149185.

Lazzari, E., Korczeniewska, J., Ní Gabhann, J., Smith, S., Barnes, B.J., and Jefferies, C.A. (2014). TRIpartite motif 21 (TRIM21) differentially regulates the stability of interferon regulatory factor 5 (IRF5) isoforms. PLoS One *9*, e103609.

Lee, Y., Collins, M., and Kuchroo, V.K. (2014). Unexpected targets and triggers of autoimmunity. J. Clin. Immunol. *34 Suppl 1* (S1), S56–S60.

Lønnberg, A.S., Zachariae, C., and Skov, L. (2014). Targeting of interleukin-17 in the treatment of psoriasis. Clin. Cosmet. Investig. Dermatol. *7*, 251–259.

Lucas, C.M., Milani, M., Butterworth, M., Carmell, N., Scott, L.J., Clark, R.E., Cohen, G.M., and Varadarajan, S. (2016). High CIP2A levels correlate with an antiapoptotic phenotype that can be overcome by targeting BCL-XL in chronic myeloid leukemia. Leukemia *30*, 1273–1281.

Mehling, M., Brinkmann, V., Antel, J., Bar-Or, A., Goebels, N., Vedrine, C., Kristofic, C., Kuhle, J., Lindberg, R.L., and Kappos, L. (2008). FTY720 therapy exerts differential effects on T cell subsets in multiple sclerosis. Neurology *71*, 1261–1267.

Meyer Zu Horste, G., Wu, C., Wang, C., Cong, L., Pawlak, M., Lee, Y., Elyaman, W., Xiao, S., Regev, A., and Kuchroo, V.K. (2016). RBPJ controls development of pathogenic Th17 cells by regulating IL-23 receptor expression. Cell Rep. *16*, 392–404.

Mi, H., Muruganujan, A., Casagrande, J.T., and Thomas, P.D. (2013). Large-scale gene function analysis with the PANTHER classification system. Nat. Protoc. *8*, 1551–1566.

Mi, H., Huang, X., Muruganujan, A., Tang, H., Mills, C., Kang, D., and Thomas, P.D. (2017). PANTHER version 11: expanded annotation data from Gene Ontology and Reactome pathways, and data analysis tool enhancements. Nucleic Acids Res. *45*, D183–D189.

Multhoff, G., Molls, M., and Radons, J. (2011). Chronic inflammation in cancer development. Front. Immunol. *2*, 98.

Ouyang, X., Zhang, R., Yang, J., Li, Q., Qin, L., Zhu, C., Liu, J., Ning, H., Shin, M.S., Gupta, M., et al. (2011). Transcription factor IRF8 directs a silencing programme for TH17 cell differentiation. Nat. Commun. *2*, 314.

Pallai, R., Bhaskar, A., Barnett-Bernodat, N., Gallo-Ebert, C., Nickels, J.T., Jr., and Rice, L.M. (2015). Cancerous inhibitor of protein phosphatase 2A promotes premature chromosome segregation and aneuploidy in prostate cancer cells through association with shugoshin. Tumor Biol. *36*, 6067–6074.

Robinson, K.M., Manni, M.L., Biswas, P.S., and Alcorn, J.F. (2013). Clinical consequences of targeting IL-17 and TH17 in autoimmune and allergic disorders. Curr. Allergy Asthma Rep. *13*, 587–595.

Romani, L. (2011). Immunity to fungal infections. Nat. Rev. Immunol. *11*, 275–288.

Saddoughi, S.A., Gencer, S., Peterson, Y.K., Ward, K.E., Mukhopadhyay, A., Oaks, J., Bielawski, J., Szulc, Z.M., Thomas, R.J., Selvam, S.P., et al. (2013). Sphingosine analogue drug FTY720 targets I2PP2A/SET and mediates lung tumour suppression via activation of PP2A-RIPK1-dependent necroptosis. EMBO Mol. Med. *5*, 105–121.

Shannon, P., Markiel, A., Ozier, O., Baliga, N.S., Wang, J.T., Ramage, D., Amin, N., Schwikowski, B., and Ideker, T. (2003). Cytoscape: a software environment for integrated models of biomolecular interaction networks. Genome Res. *13*, 2498–2504.

Shentu, Y.-P., Huo, Y., Feng, X.L., Gilbert, J., Zhang, Q., Liuyang, Z.Y., Wang, X.L., Wang, G., Zhou, H., Wang, X.C., et al. (2018). CIP2A causes Tau/APP phosphorylation, synaptopathy, and memory deficits in alzheimer's disease. Cell Rep. *24*, 713–723.

Subramanian, A., Tamayo, P., Mootha, V.K., Mukherjee, S., Ebert, B.L., Gillette, M.A., Paulovich, A., Pomeroy, S.L., Golub, T.R., Lander, E.S., and Mesirov, J.P. (2005). Gene set enrichment analysis: a knowledge-based approach for interpreting genome-wide expression profiles. Proc. Natl. Acad. Sci. U S A *102*, 15545–15550.

Switzer, C.H., Cheng, R.Y.S., Vitek, T.M., Christensen, D.J., Wink, D.A., and Vitek, M.P. (2011). Targeting SET/I2PP2A oncoprotein functions as a multi-pathway strategy for cancer therapy. Oncogene *30*, 2504–2513.

Szklarczyk, D., Morris, J.H., Cook, H., Kuhn, M., Wyder, S., Simonovic, M., Santos, A., Doncheva, N.T., Roth, A., Bork, P., et al. (2017). The STRING database in 2017: quality-controlled protein-protein association networks, made broadly accessible. Nucleic Acids Res. *45*, D362–D368.

Tripathi, S.K., Chen, Z., Larjo, A., Kanduri, K., Nousiainen, K., Äijo, T., Ricaño-Ponce, I., Hrdlickova, B., Tuomela, S., Laajala, E., et al. (2017). Genome-wide analysis of STAT3-mediated transcription during early human Th17 cell differentiation. Cell Rep. *19*, 1888–1901.

Tripathi, S.K., Välikangas, T., Shetty, A., Khan, M.M., Moulder, R., Bhosale, S.D., Komsi, E., Salo, V., De Albuquerque, R.S., Rasool, O., et al. (2019). Quantitative proteomics reveals the dynamic protein landscape during initiation of human Th17 cell polarization. iScience *11*, 334–355.

Tuomela, S., Rautio, S., Ahlfors, H., Öling, V., Salo, V., Ullah, U., Chen, Z., Hämälistö, S., Tripathi, S.K., Äijö, T., et al. (2016). Comparative analysis of human and mouse transcriptomes of Th17 cell priming. Oncotarget *7*, 13416–13428.

Ubaid Ullah, U., Andrabi, S.B.A., Tripathi, S.K., Dirasantha, O., Kanduri, K., Rautio, S., Gross, C.C., Lehtimäki, S., Bala, K., Tuomisto, J., et al. (2018). Transcriptional repressor HIC1 contributes to suppressive function of human induced regulatory T cells. Cell Rep. *22*, 2094–2106.

Ventelä, S., Côme, C., Mäkelä, J.A., Hobbs, R.M., Mannermaa, L., Kallajoki, M., Chan, E.K., Pandolfi, P.P., Toppari, J., and Westermarck, J. (2012). CIP2A promotes proliferation of spermatogonial progenitor cells and spermatogenesis in mice. PLoS One *7*, e33209.

Vizcaíno, J.A., Csordas, A., Del-Toro, N., Dianes, J.A., Griss, J., Lavidas, I., Mayer, G., Perez-Riverol, Y., Reisinger, F., Ternent, T., et al. (2016). 2016 update of the PRIDE database and its related tools. Nucleic Acids Res. *44*, D447–D456.

Wang, J., Okkeri, J., Pavic, K., Wang, Z., Kauko, O., Halonen, T., Sarek, G., Ojala, P.M., Rao, Z., Xu, W., and Westermarck, J. (2017). Oncoprotein CIP2A is stabilized via interaction with tumor suppressor PP2A/B56. EMBO Rep. *18*, 437–450.

Wu, C., Yosef, N., Thalhamer, T., Zhu, C., Xiao, S., Kishi, Y., Regev, A., and Kuchroo, V.K. (2013). Induction of pathogenic TH17 cells by inducible salt-sensing kinase SGK1. Nature *496*, 513–517.

Xiao, S., Yosef, N., Yang, J., Wang, Y., Zhou, L., Zhu, C., Wu, C., Baloglu, E., Schmidt, D., Ramesh, R., et al. (2014). Small-molecule RORγt antagonists inhibit T helper 17 cell transcriptional network by divergent mechanisms. Immunity *40*, 477–489.

Xu, T., Wang, X., Zhong, B., Nurieva, R.I., Ding, S., and Dong, C. (2011). Ursolic acid suppresses interleukin-17 (IL-17) production by selectively antagonizing the function of RORgamma t protein. J. Biol. Chem. *286*, 22707–22710.

Xu, Q., Jin, X., Zheng, M., Rohila, D., Fu, G., Wen, Z., Lou, J., Wu, S., Sloan, R., Wang, L., et al. (2019). Phosphatase PP2A is essential for TH17 differentiation. Proc. Natl. Acad. Sci. U S A *116*, 982–987.

Yang, K., Shi, H.X., Liu, X.Y., Shan, Y.F., Wei, B., Chen, S., and Wang, C. (2009). TRIM21 is essential to sustain IFN regulatory factor 3 activation during antiviral response. J. Immunol. *182*, 3782–3792.

Yang, X., Zhang, Y., Liu, H., and Lin, Z. (2016). Cancerous inhibitor of PP2A silencing inhibits proliferation and promotes apoptosis in human multiple myeloma cells. Biomed. Res. Int. *2016*, 6864135.

Yosef, N., Shalek, A.K., Gaublomme, J.T., Jin, H., Lee, Y., Awasthi, A., Wu, C., Karwacz, K., Xiao, S., Jorgolli, M., et al. (2013). Dynamic regulatory network controlling TH17 cell differentiation. Nature *496*, 461–468.

Yoshimi, R., Ishigatsubo, Y., and Ozato, K. (2012). Autoantigen TRIM21/Ro52 as a possible target for treatment of systemic lupus erythematosus. Int. J. Rheumatol. *2012*, 718237.

Yu, H.-C., Hou, D.R., Liu, C.Y., Lin, C.S., Shiau, C.W., Cheng, A.L., and Chen, K.F. (2013). Cancerous inhibitor of protein phosphatase 2A mediates bortezomib-induced autophagy in hepatocellular carcinoma independent of proteasome. PLoS One *8*, e55705.

iScience, Volume *23*

Supplemental Information

CIP2A Constrains Th17 Differentiation by Modulating STAT3 Signaling

Mohd Moin Khan, Ubaid Ullah, Meraj H. Khan, Lingjia Kong, Robert Moulder, Tommi Välikangas, Santosh Dilip Bhosale, Elina Komsi, Omid Rasool, Zhi Chen, Laura L. Elo, Jukka Westermarck, and Riitta Lahesmaa

Figure S1 (Related to Figure 1)

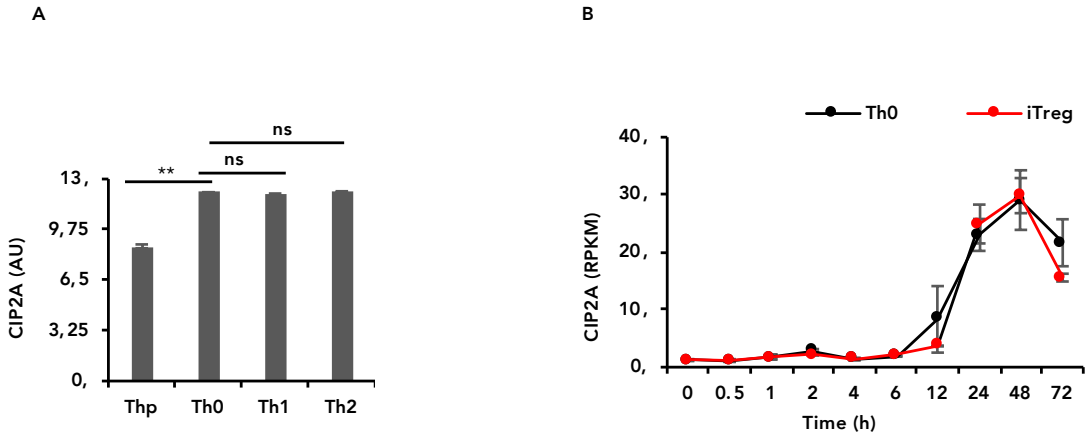

Figure S1 CIP2A Expression in Human T helper Cells. Related to Figure1.
(A-B) Data from earlier published studies showing CIP2A expression in (A) unactivated human naïve precursor CD4+ T-cells (Thp), Th0, Th1 and Th2 cells at 72 h following cell activation (microarray data: Kanduri et al. 2015) and (B) in human iTreg and Th0 control cells at the indicated timepoints post cell activation (RNA-Seq data from Ullah et al., 2018).

Figure S2 (Related to Figure 2)

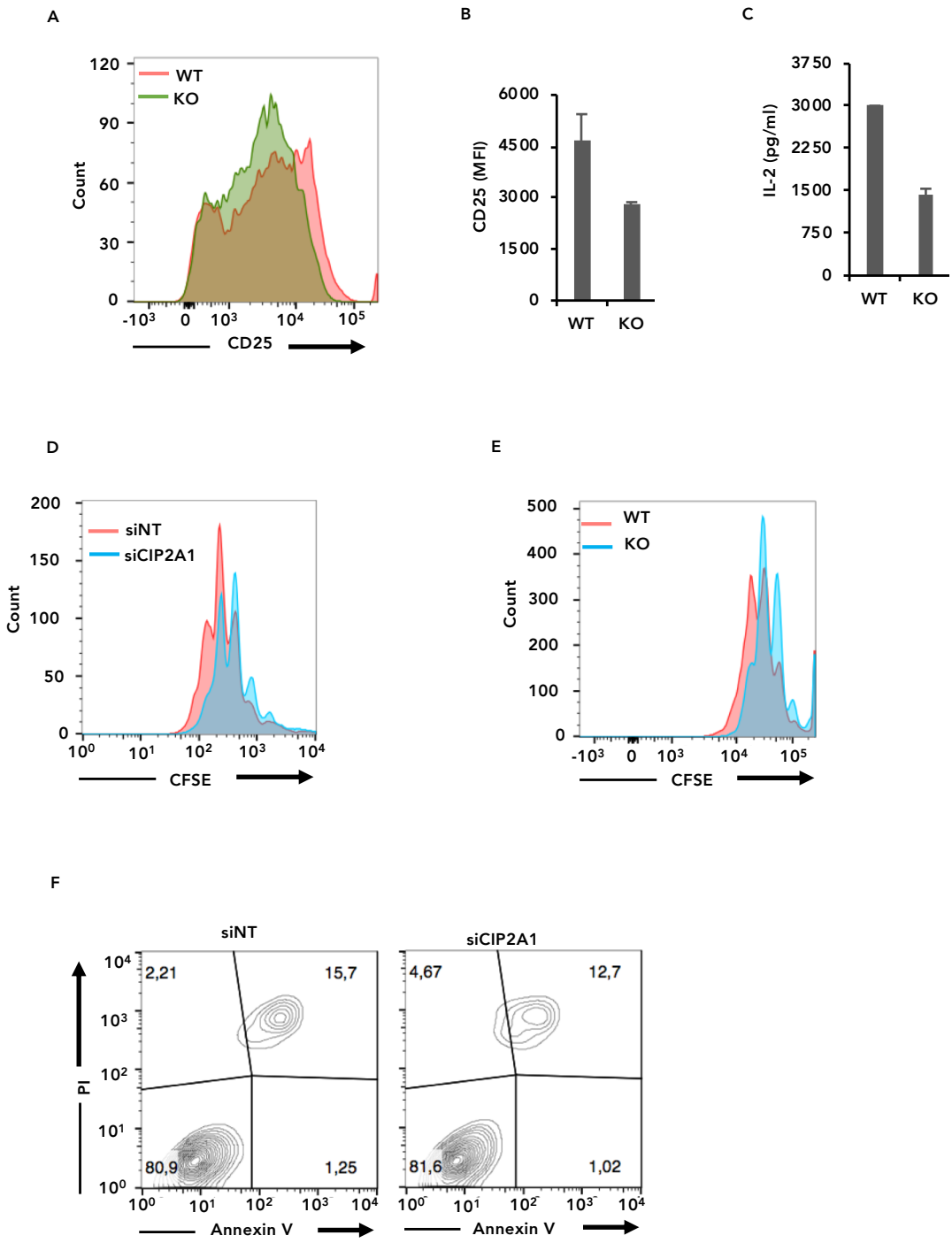

Figure S2 CIP2A Deficiency Leads to Altered Proliferation and T Cell Activation. Related to Figures 2 and 3.

(A) Analysis of CD25 expression on the surface of activated mouse CD4+ cells. Red and green colour denote cells from wild-type (WT) and CIP2A knockout (KO) mice, respectively.

(B) Average MFI of two independent biological replicates of the experiments shown in (A).

(C) Measurement of IL-2 secretion by Luminex in CIP2A deficient mouse Th17 cells. The bar charts show the mean of three biological replicates.

(D) Analysis of cell proliferation in CIP2A silenced and control human cells after four days of differentiation under Th17 conditions. Red and blue colours represent cells treated with siNT or siCIP2A1, respectively. This is a representative of two biological replicates. (E) Analysis of cell proliferation in CIP2A WT and KO mouse cells after four days of differentiation under Th17 conditions. Red and blue colours represent cells from WT and KO mice, respectively. (F) Analysis of live cells in the siRNA treated human Th17 cells with Annexin-V and PI. Live cells are double negative. This is an example of three biological replicates.

Figure S3 (Related to Figure 4)

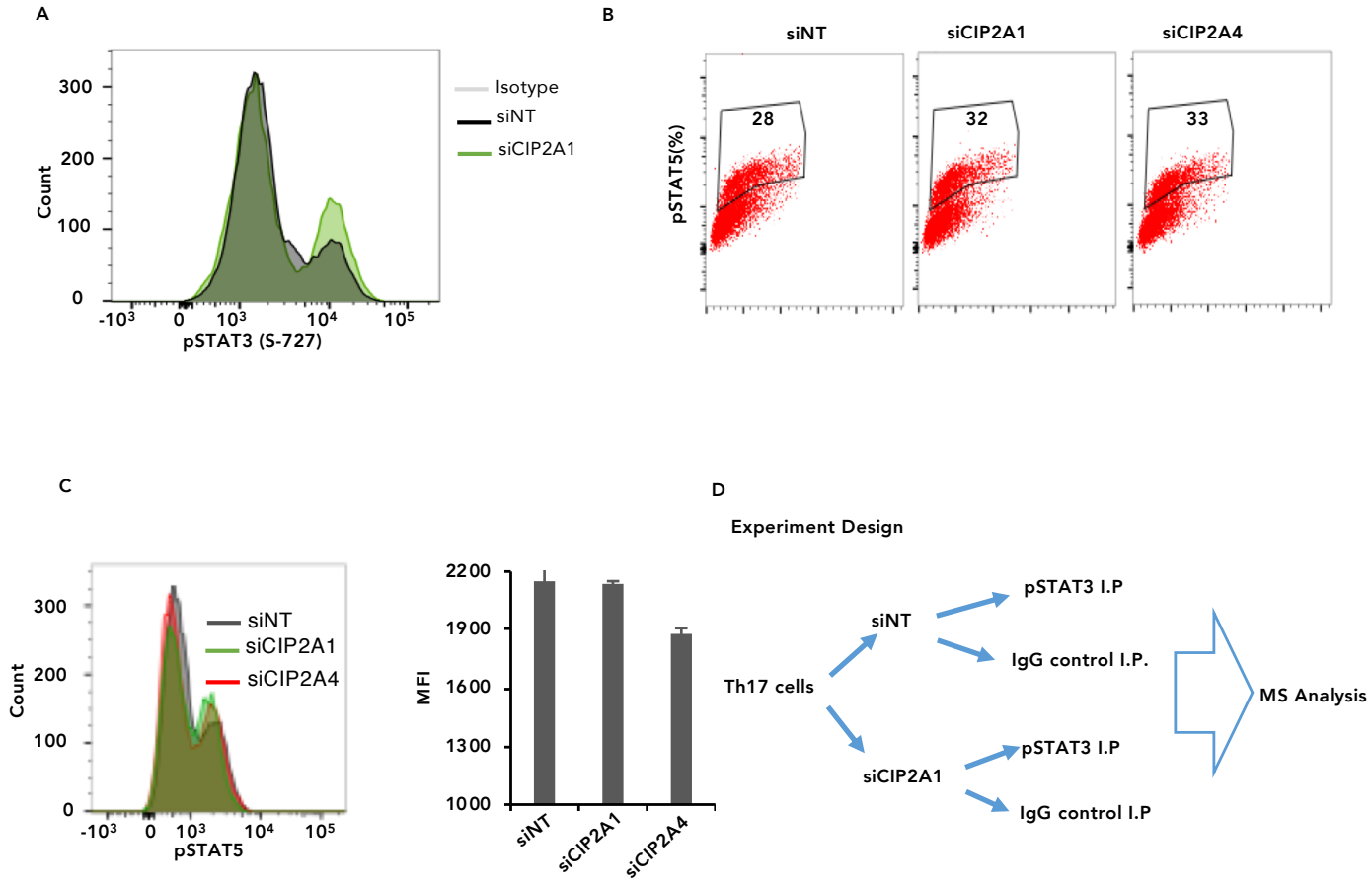

Figure S3. Effect of CIP2A Silencing on STAT3 and STAT5 Phosphorylation in Human Th17 and iTreg cells, respectively. Related to Figure 4.
(A) Flow cytometry analysis of pSTAT3 (S727) in cells nucleofected with siCIP2A1 (green) or siNT (black) siRNA in culturing conditions as in Figure 4B. Grey colour represents isotype control.
(B-C) Flow cytometry analysis of pSTAT5 phosphorylation (Y694) in cells nucleofected with siCIP2A1 (green), siCIP2A4 (red) and siNT (black) siRNA as described previously in Figure 4B, except that the cells were activated and reactivated under iTreg culturing conditions. The bar chart shows quantitation of MFI of three independent experiments.
(D) Experimental design for immunoprecipitation with anti p-STAT3 (Y705) in CIP2A silenced and control
human Th17 cells. IgG control antibodies were used as a negative control in both conditions. CD4+ T cells were isolated from human umbilical cord blood and activated first in Th17 condition for 48 h. Cells were then nucleofected with CIP2A or NT siRNAs, rested for 48 h and then reactivated again under Th17 culturing condition for 15 min followed by pSTAT3 pulldowns.

Figure S4 (Related to Figure 5)

A

Top canonical pathways	siNT	siCIP2A
Remodeling of Epithelial Adherens Junctions	9.83E-12	1.15E-09
EIF2 Signaling	2.96E-10	
Regulation of Actin-based Motility by Rho	3.75E-10	2.35E-08
CD28 Signaling in T Helper Cells	4.45E-10	
Actin Cytoskeleton Signaling	6.48E-10	
Protein Kinase A Signaling		1.62E-09
Epithelial Adherens Junction Signaling		8.27E-09
Breast Cancer Regulation by Stathmin1		1.51E-08

B

Top associated network functions	siNT	siCIP2A
Cell Morphology, Cellular Function and Maintenance, DNA Replication, Recombination, and Repair	47	
Cellular Assembly and Organization, Cell-To-Cell Signaling and Interaction, Reproductive System Development and Function	42	43
Protein Synthesis, RNA Post-Transcriptional Modification, Gene Expression	42	
Cell Signaling, Molecular Transport, Vitamin and Mineral Metabolism	38	
Cell Signaling, Post-Translational Modification, Cell-To-Cell Signaling and Interaction		34
Cancer, Organismal Injury and Abnormalities, Renal and Urological Disease and Repair	18	
RNA Post-Transcriptional Modification, Cell Cycle, DNA Replication, Recombination,		48
RNA Post-Transcriptional Modification, Cancer, Gastrointestinal Disease		26
Cellular Movement, Connective Tissue Development and Function, Cell Morphology		23

C

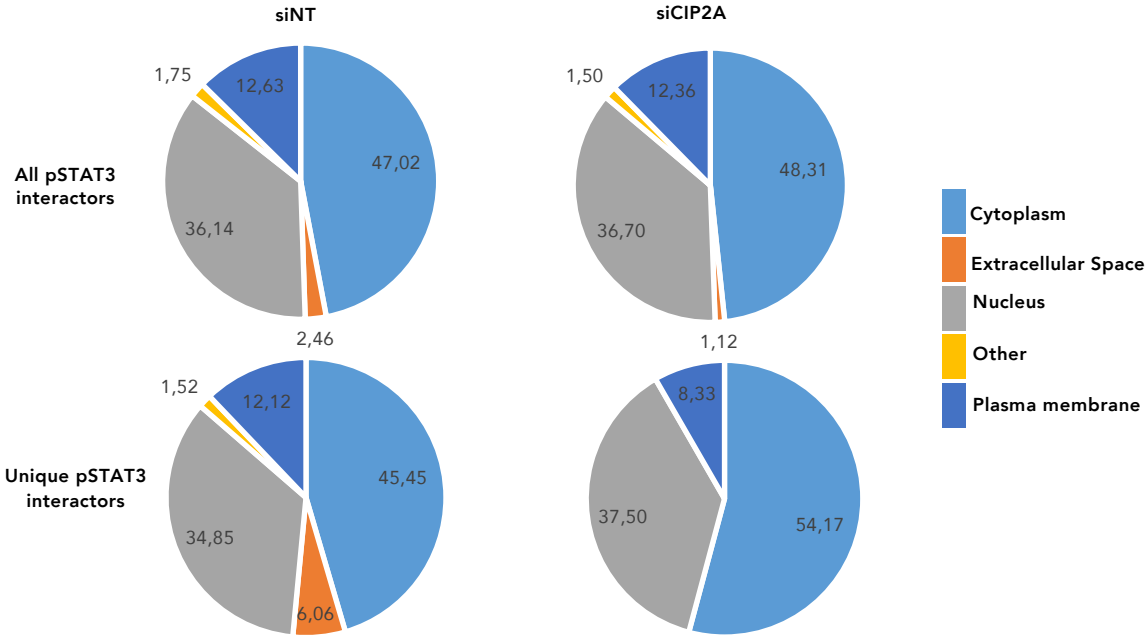

D

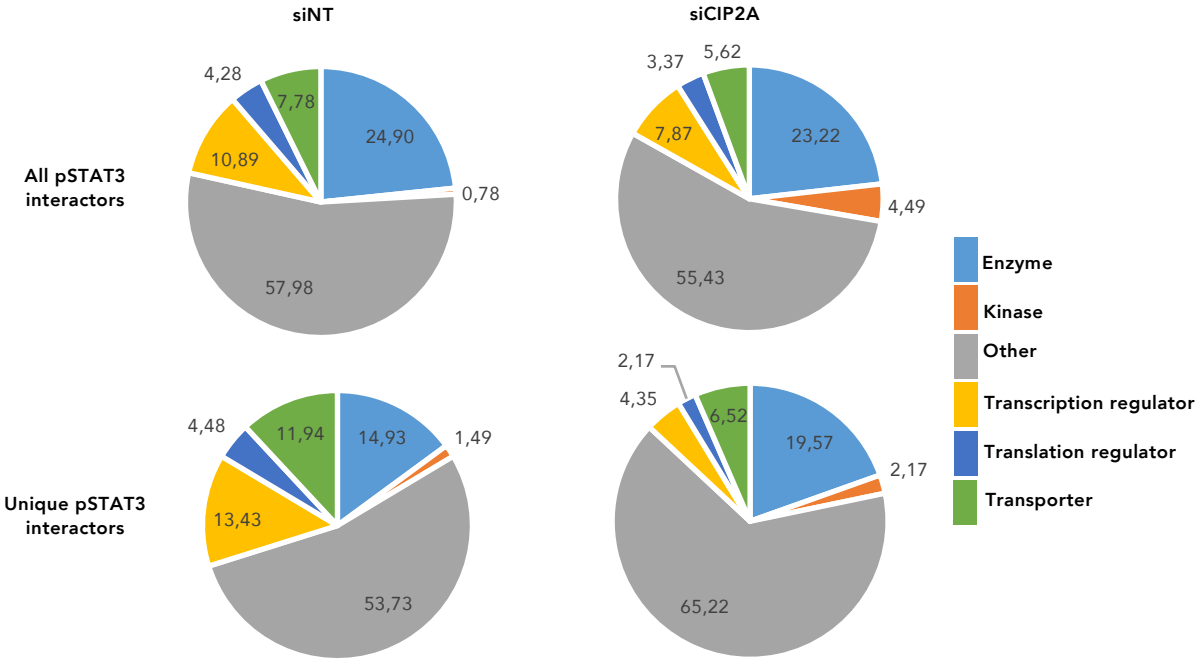

Figure S4. STAT3 Interactome Ingenuity Pathway Analysis (IPA) in CIP2A Silenced Human Th17 cells. Related to Figure 5.
(A) Top IPA pathways enriched in pSTAT3 interactors in siNT and siCIP2A1 treated cells.
(B) Top 5 associated network function in IPA analysis of preferentially interacting proteins with STAT3. The lists of proteins were analyzed using IPA with the full human genome/proteome as a background.
(C) Cellular location of pSTAT3 interactors under siNT or siCIP2A1 treated cells are shown as a Venn diagram. The top panel shows the data for all the interactors while the bottom panel shows the data for the interactors that preferentially interact under siNT or siCIP2A1 condition.
(D) Functional classification of pSTAT3 interactors under siNT or siCIP2A1 treated cells are shown as a Venn diagram. The top panel shows the data for all the interactors while the bottom panel shows the data for the interactors that preferentially interact under siNT or siCIP2A1 condition.

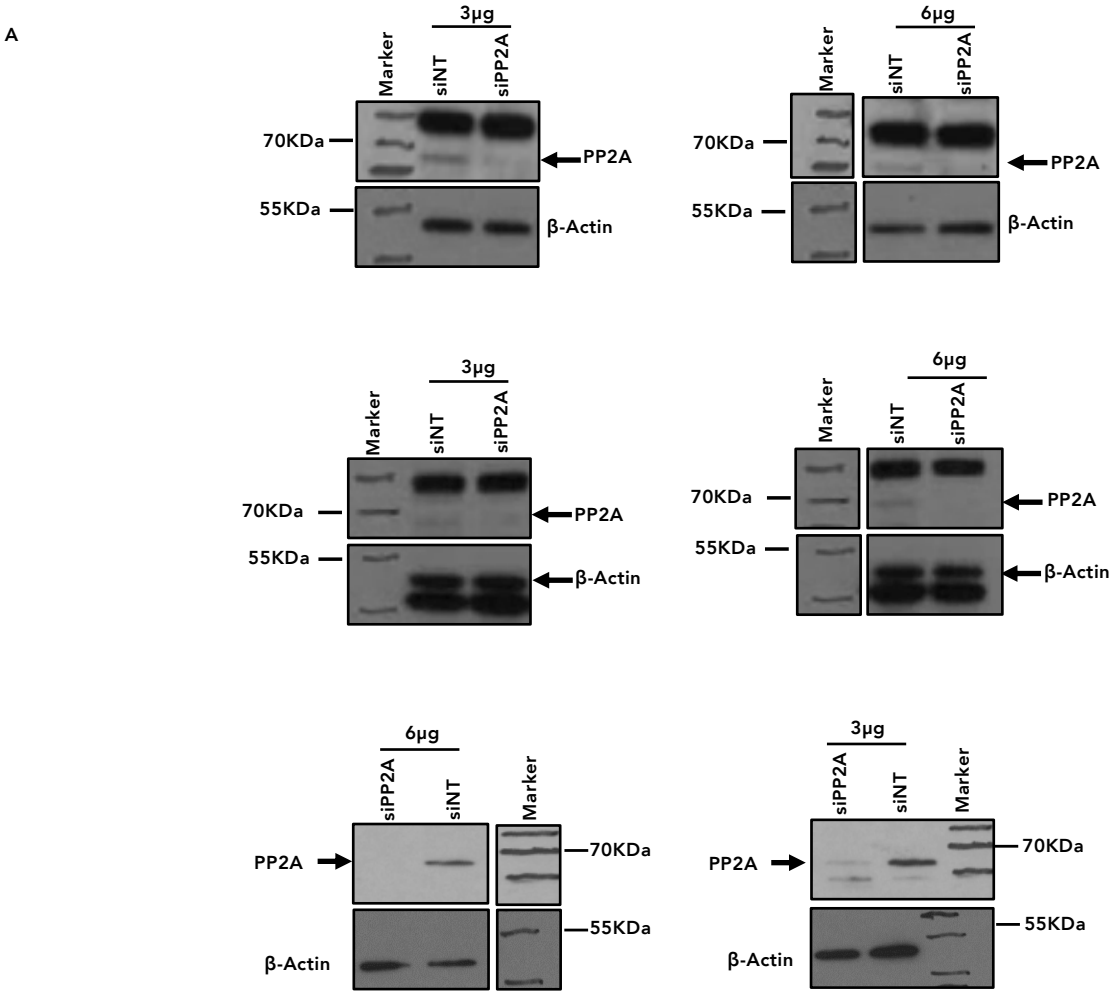

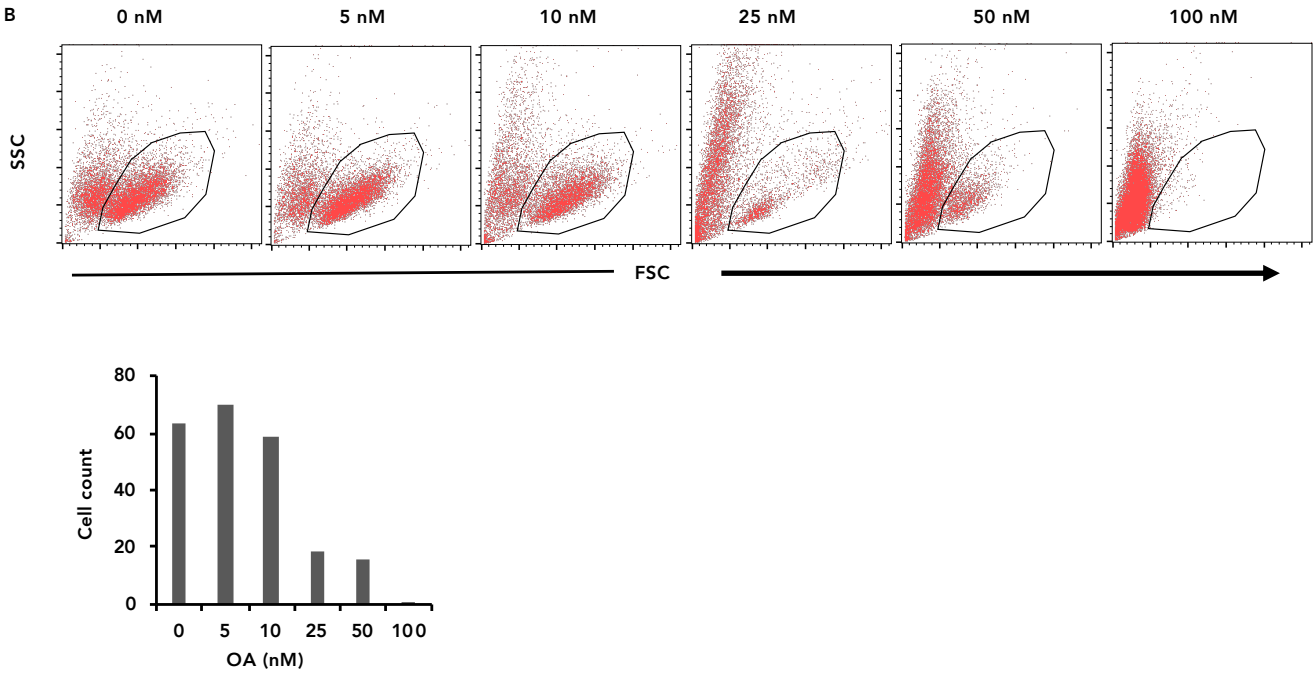

Figure S5. PP2A inhibition in human Th17 cells. Related to Figure 7.
(A) Additional three replicates of WB analysis in PP2A silenced Th17 cells (Replicate 4 is representative WB in Figure 7A). Two different amounts (3ug and 6ug) of PP2A siRNA were used to deplete PP2A in human Th17 cells. Beta-actin was used to probe equal loading of lysates. In the PP2A blots, the upper bands in replicate 1-2 and lower bands in replicate 4 (Figure 7A) are non-specific.
(B) Flow cytometry dot blot (top) and bar graph (bottom) plotted with flow cytometry cell count at 72h in Th17 cells with shown concentration of OA.

Supplementary Table S1

Genes DE upon CIP2A silencing. (Associated with Fig. 3). The table lists genes that were detected as differential expressed in the comparison of the RNA-seq data from Th17 cells treated with CIP2A siRNA compared to those treated with scramble. An FDR of 0.05 and fold change cut-off was applied.

gene	logFC	logCPM	LR	PValue	FDR
ABCB6	0,54	2,54	14,32	0,00015	0,04414
ACSL5	-0,31	4,86	13,92	0,00019	0,04986
ANXA1	-0,47	4,37	24,23	0,00000	0,00115
APRT	-0,28	7,86	30,03	0,00000	0,00009
AQP3	0,45	5,20	27,37	0,00000	0,00031
ATHL1	0,44	6,21	39,41	0,00000	0,00000
ATP2B4	0,41	4,39	19,01	0,00001	0,00901
ATP8A1	0,19	6,68	14,35	0,00015	0,04414
CCDC86	-0,18	7,22	14,97	0,00011	0,03496
CCL22	0,49	4,74	37,06	0,00000	0,00000
CCL4	0,26	6,71	25,17	0,00000	0,00082
CCNA2	0,33	5,30	16,52	0,00005	0,02007
CCR7	0,20	7,42	14,31	0,00016	0,04415
CD200	-0,20	7,66	19,13	0,00001	0,00887
CD320	-0,23	7,01	15,92	0,00007	0,02442
CLPP	-0,19	6,73	15,48	0,00008	0,02935
CPM	-0,27	6,04	21,75	0,00000	0,00324
CPNE1	-0,19	6,94	17,84	0,00002	0,01295
CPXM1	0,91	2,06	18,42	0,00002	0,01094
CREBBP	-0,18	6,46	13,98	0,00018	0,04978
CSF2	-0,18	7,31	14,89	0,00011	0,03553
CTD-2020K17.1	0,50	3,67	16,31	0,00005	0,02068
CXCL12	0,84	2,12	24,57	0,00000	0,00106
CXCR4	0,34	4,58	16,39	0,00005	0,02060
CYP1A1	0,29	4,71	14,16	0,00017	0,04622
DDX49	-0,20	6,82	20,61	0,00001	0,00527
DICER1	-0,19	7,05	16,39	0,00005	0,02060
DUSP6	0,24	5,40	14,07	0,00018	0,04780
DYNLRB1	-0,24	5,72	17,23	0,00003	0,01571
EXOSC5	-0,25	5,31	13,92	0,00019	0,04986
FAM111A	0,35	5,48	19,34	0,00001	0,00812
FAM49A	0,51	3,49	17,94	0,00002	0,01265
FAM96B	-0,21	6,62	17,20	0,00003	0,01571
FNBP1L	0,25	6,20	15,36	0,00009	0,03030
FNDC9	0,55	3,31	22,44	0,00000	0,00241
FOXM1	0,31	4,76	14,82	0,00012	0,03631
G0S2	-0,33	6,43	32,71	0,00000	0,00003
GALNT10	0,17	6,74	13,92	0,00019	0,04986
GBP4	-0,36	4,97	24,46	0,00000	0,00108
GBP5	-0,33	4,41	16,29	0,00005	0,02068
GLRX	0,46	3,43	14,21	0,00016	0,04527
GSTP1	-0,20	7,39	17,81	0,00002	0,01297
GXYLT1	0,29	5,20	14,66	0,00013	0,03868
HMGB2	0,22	6,34	16,09	0,00006	0,02261
HPGD	0,41	3,81	14,80	0,00012	0,03632
IER3	-0,43	8,56	46,09	0,00000	0,00000
IFNG	-0,33	5,74	17,67	0,00003	0,01356
IGHM	0,45	3,62	16,48	0,00005	0,02007
IRF8	-0,38	7,92	42,17	0,00000	0,00000
ITGAE	0,25	5,52	16,28	0,00005	0,02068
J01415.22	0,51	3,91	19,75	0,00001	0,00748
J01415.23	0,35	7,78	18,69	0,00002	0,00996
KIAA1524	-2,17	4,69	482,41	0,00000	0,00000
KIF1A	0,62	2,66	16,89	0,00004	0,01719
LIMA1	0,37	4,71	17,00	0,00004	0,01680
LMLN	-0,95	3,91	71,65	0,00000	0,00000

LOXL3	0,57	2,51	15,34	0,00009	0,03036
MAF	0,35	5,15	21,46	0,00000	0,00357
MALAT1	0,57	6,89	18,16	0,00002	0,01205
MAP1A	0,47	4,64	31,17	0,00000	0,00006
MCAM	0,50	4,18	24,19	0,00000	0,00115
MEX3C	-0,21	7,34	23,59	0,00000	0,00146
MIAT	0,92	4,09	44,76	0,00000	0,00000
MLL2	-0,21	7,49	14,24	0,00016	0,04491
MRPL14	-0,33	5,18	19,47	0,00001	0,00811
MRPL4	-0,20	6,68	17,62	0,00003	0,01373
MYH10	0,45	4,26	17,34	0,00003	0,01543
NCS1	0,23	6,24	17,96	0,00002	0,01265
NDC80	0,42	4,00	17,89	0,00002	0,01282
NEAT1	0,50	6,95	25,14	0,00000	0,00082
NFKBID	-0,17	6,92	14,33	0,00015	0,04414
NIPAL4	0,37	4,52	16,85	0,00004	0,01733
NME1	-0,20	7,35	18,76	0,00001	0,00978
NUTF2	-0,23	6,30	17,18	0,00003	0,01571
P2RY8	0,29	5,55	14,54	0,00014	0,04036
PABPC1L	0,38	4,95	17,22	0,00003	0,01571
PALLD	0,36	6,45	42,57	0,00000	0,00000
PARP2	0,24	5,42	14,07	0,00018	0,04780
PHLDA1	-0,24	5,74	16,29	0,00005	0,02068
PLCB2	0,27	5,67	16,94	0,00004	0,01718
PNISR	0,23	7,03	15,50	0,00008	0,02927
PNMA2	1,46	0,48	19,43	0,00001	0,00811
POLR3H	-0,24	6,62	23,62	0,00000	0,00146
PPDPF	-0,29	5,55	18,09	0,00002	0,01226
PPP1R14B	-0,20	7,87	15,04	0,00011	0,03401
PQLC1	-0,27	5,23	16,90	0,00004	0,01719
PRDX2	-0,19	7,13	18,60	0,00002	0,01021
PRKX	-0,39	5,15	30,48	0,00000	0,00009
PRMT6	-0,24	5,67	15,43	0,00009	0,02977
PSMB8	-0,20	6,94	18,95	0,00001	0,00901
RAVER1	-0,20	6,51	15,78	0,00007	0,02586
RHOG	-0,21	7,06	25,23	0,00000	0,00082
RMRP	1,42	0,65	22,61	0,00000	0,00236
RN7SK	0,78	1,83	17,50	0,00003	0,01435
RORA	0,26	5,93	22,52	0,00000	0,00239
RORC	0,32	6,06	35,28	0,00000	0,00001
RP11-326C3.2	0,46	3,37	15,38	0,00009	0,03030
RP5-882C2.2	2,08	-0,83	17,11	0,00004	0,01605
RPS28	-0,23	7,99	18,41	0,00002	0,01094
RPTOR	-0,20	7,60	18,18	0,00002	0,01205
RRM2	0,30	7,27	27,60	0,00000	0,00029
RYR1	0,23	6,38	15,75	0,00007	0,02589
S100A4	0,35	4,86	20,19	0,00001	0,00609
SCAND1	-0,33	4,94	17,77	0,00002	0,01306
SDC4	-0,22	7,77	20,36	0,00001	0,00571
SEC31B	0,47	3,65	16,49	0,00005	0,02007
SF3A2	-0,19	6,59	15,30	0,00009	0,03072
SH2D1A	0,24	5,38	14,94	0,00011	0,03527
SH3BGRL3	-0,24	8,33	14,64	0,00013	0,03868
SLAMF7	-0,27	5,37	16,74	0,00004	0,01816
SLC25A23	-0,34	4,64	18,01	0,00002	0,01261
SLC25A39	-0,19	7,16	19,38	0,00001	0,00811
SLC25A44	-0,28	6,14	21,46	0,00000	0,00357
SNORD3A	1,49	1,25	48,13	0,00000	0,00000
SPOCK2	0,23	7,15	29,23	0,00000	0,00013
SSNA1	-0,21	6,41	15,05	0,00010	0,03401
SSTR3	0,64	2,63	16,28	0,00005	0,02068

TAF1D	0,20	7,82	14,63	0,00013	0,03868
TAGAP	-0,21	7,72	21,15	0,00000	0,00407
TET3	-0,30	4,76	15,89	0,00007	0,02454
TIMM13	-0,23	6,63	15,22	0,00010	0,03185
TMCC2	-0,25	5,86	18,98	0,00001	0,00901
TNFRSF10C	5,55	-2,71	15,14	0,00010	0,03292
TNFRSF4	-0,22	7,82	19,05	0,00001	0,00901
TNFSF8	-0,34	5,37	25,84	0,00000	0,00066
TNPO2	-0,23	8,17	19,38	0,00001	0,00811
TOP2A	0,27	5,83	14,84	0,00012	0,03626
TSTA3	-0,29	7,06	43,51	0,00000	0,00000
TUBA1A	0,28	6,22	22,36	0,00000	0,00243
UBASH3B	0,26	5,39	17,24	0,00003	0,01571
UBE2M	-0,16	7,10	13,93	0,00019	0,04986
UST	1,27	0,61	20,38	0,00001	0,00571
WIPF1	-0,18	6,84	14,89	0,00011	0,03553
WSB1	0,28	6,02	14,26	0,00016	0,04491
XIRP1	-0,45	4,48	30,17	0,00000	0,00009
ZNF135	1,56	0,26	19,44	0,00001	0,00811

Supplementary Table S2.
Fifty CIP2A regulated genes that are DE during human Th17 cell differentiation.(Associated to Fig. 3)
On the basis of the data of Tuomela et al. 2016, fifty of 136 genes DE upon CIP2A silencing were are also observed as DE during Th17 differentiation. The data from the Tuomela et al. publication is shown for these 50 genes for eight time points in the first 72 hours of differentiation (0.5, 1, 2, 4, 6, 12, 24, 48 & 72 hours).

	data from this study	The data is taken from Tuomela S et al. 2016.								
Gene	Log FC_siNT_siCIP2A1	log FC_0.5h	log FC_1h	log FC_2h	log FC_4h	log FC_6h	log FC_12h	log FC_24h	log FC_48h	log FC_72h
ANXA1	-0,47	0,11	0,00	-0,08	-0,41	-0,50	-1,07	-1,60	-1,76	-1,39
AQP3	0,45	-0,19	-0,12	0,01	-0,55	-0,08	0,48	1,38	2,87	2,06
ATHL1	0,44	-0,31	-0,21	-0,16	-0,53	-0,48	-0,63	-0,40	-1,12	-1,15
ATP2B4	0,41	-0,05	0,12	1,40	1,02	1,32	0,91	1,69	1,24	0,88
ATP8A1	0,19	0,17	0,07	0,28	1,19	1,61	1,24	0,61	0,57	0,36
CCL22	0,49	-0,40	-1,12	1,18	1,88	1,02	1,93	3,35	2,76	2,47
CCL4	0,26	0,39	1,39	0,27	-0,52	-0,10	0,08	2,66	2,49	0,07
CD200	-0,20	-0,06	0,32	-0,46	-1,47	-0,64	-1,02	-1,58	-0,63	0,20
CPM	-0,27	0,54	-1,17	0,43	0,42	0,16	-0,70	-1,85	-1,22	-0,30
CPXM1	0,91	-0,56	0,11	0,01	0,08	0,14	0,23	0,24	0,26	1,06
CSF2	-0,18	0,81	0,95	0,57	-1,38	-0,16	1,05	1,11	-0,29	-3,47
CYP1A1	0,29	4,35	0,89	-0,26	-1,24	-0,56	-0,27	1,09	0,11	-0,28
DUSP6	0,24	-0,13	-0,34	0,29	-0,34	0,54	0,88	1,06	0,55	-0,03
FAM49A	0,51	-0,18	0,10	-0,64	-0,76	-0,01	1,12	1,31	0,72	1,11
FNBP1L	0,25	0,08	0,03	0,14	-0,26	0,28	1,48	4,31	4,75	4,37
FNDC9	0,55	-0,01	-0,21	0,33	-0,78	0,39	0,74	4,05	4,22	3,35
G0S2	-0,33	0,15	0,94	-0,82	-0,24	-0,33	-0,21	-1,42	-0,88	0,28
GALNT10	0,17	0,04	0,07	0,11	0,13	0,32	0,89	1,27	1,67	1,95
GBP4	-0,36	0,38	1,04	2,11	2,68	2,00	1,23	0,94	-0,72	-1,63
GBP5	-0,33	0,09	0,97	1,92	1,05	0,41	-0,59	-0,62	-1,99	-2,64
GLRX	0,46	0,58	1,28	0,96	0,26	0,07	0,04	0,13	0,00	-0,02
IER3	-0,43	0,76	-0,06	-1,09	-2,41	-1,30	-0,84	-0,42	-0,02	0,91
IFNG	-0,33	1,07	-0,11	-0,82	-0,12	0,62	1,30	1,08	0,93	-0,92
IGHM	0,45	-0,18	0,02	0,23	-0,24	-0,08	0,04	-1,29	-2,19	-1,97
IRF8	-0,38	0,50	1,63	0,95	-0,87	-0,43	-0,59	-1,84	-0,57	-0,77

ITGAE	0,25	-0,03	-0,17	0,13	0,44	0,05	-0,03	0,94	2,84	3,09
KIF1A	0,62	0,24	1,33	0,85	-0,15	0,54	1,48	3,35	2,74	2,07
LIMA1	0,37	0,11	0,29	-0,52	-1,19	-0,58	-0,66	-0,70	-0,07	0,02
LOXL3	0,57	-0,88	-0,41	0,95	-0,70	0,00	0,45	3,07	3,20	3,19
MAF	0,35	0,24	0,86	1,74	1,49	1,74	1,97	1,32	1,29	1,48
MAP1A	0,47	-0,08	0,07	0,08	-0,41	0,12	0,57	1,69	0,96	1,20
MCAM	0,50	-0,20	-0,24	-0,53	-0,38	-0,06	0,52	0,82	1,08	1,31
MIAT	0,92	0,17	0,23	2,36	3,16	3,41	2,99	2,41	2,05	2,04
NCS1	0,23	-1,56	3,10	1,83	0,75	1,75	2,05	2,92	3,71	2,91
NEAT1	0,50	0,33	0,33	1,02	0,46	0,88	0,36	0,38	-0,98	-0,61
NFKBID	-0,17	0,09	-0,74	-0,57	-2,03	-1,00	-0,56	-0,38	0,11	0,55
NIPAL4	0,37	0,29	1,10	0,61	-0,13	1,07	2,06	3,11	4,23	4,20
PALLD	0,36	0,41	0,53	0,22	-0,43	0,72	3,06	3,45	2,50	1,94
PHLDA1	-0,24	-0,11	-0,50	-0,53	-1,26	-0,76	-1,94	-2,36	-1,83	-2,18
RORA	0,26	0,11	-0,01	-0,32	1,14	1,19	1,96	1,60	1,94	1,77
RORC	0,32	-1,14	0,00	-0,80	0,50	1,89	3,16	5,30	5,53	5,82
RP11-326C3.	0,46	-0,28	-0,36	-0,21	-0,55	-0,46	-0,67	-0,43	-1,20	-1,13
RRM2	0,30	1,05	0,48	-0,51	-1,00	-0,44	0,17	0,82	0,29	-0,06
RYR1	0,23	-0,21	0,27	0,27	0,07	0,14	0,97	3,52	3,53	3,69
S100A4	0,35	0,03	0,10	-0,65	-1,20	-1,11	-0,05	0,15	0,34	0,02
SDC4	-0,22	-0,70	-0,39	-0,36	-0,84	-0,61	-0,04	0,71	1,55	1,15
SSTR3	0,64	-0,28	0,02	0,01	-0,11	0,00	0,43	0,46	1,25	1,84
TNFRSF10C	5,55	0,02	1,45	2,07	-1,32	-1,01	-1,62	-0,50	-0,98	-0,78
TNFSF8	-0,34	0,01	0,27	0,47	-0,69	-0,27	-0,59	-2,53	-3,07	-2,86
WIPF1	-0,18	-0,05	-0,02	-0,04	-0,04	-0,12	-0,45	-0,74	-1,25	-1,03

Supplementary Table S3. Transcription Factor Binding site Analysis for the promoters of the DE genes. (Related to Fig. 3).Enriched motifs are shown in the first column. FDR<0.05 was considered significant. "Yes and No" column shows the likelihood of TFBS in the test set as compared to background set.

Enriched motifs	FactorName	PValue	Yes	No	Yes_No	FDR
V$HOMEZ_01	**Homez**	6,29E-80	16,69	13,9542	1,20	2,26E-77
V$GATA3_12	**GATA-3**	8,12E-63	27,27	19,2748	1,42	1,46E-60
V$HMBOX1_01	**Hmbox1**	2,39E-45	18,15	13	1,40	2,86E-43
V$ARID3A_02	**ARID3A**	1,27E-39	4,66	4,5573	1,02	1,14E-37
V$REST_14	**REST**	1,25E-28	21,81	13,8779	1,57	8,97E-27
V$EGR2_Q6	**Egr-2**	3,29E-28	3,34	0,3817	8,74	1,97E-26
V$CREBP1_01	**ATF-2**	2,30E-24	3,47	3,1756	1,09	1,18E-22
V$BCL6_01	**BCL6**	1,97E-20	2,92	0,4122	7,09	8,85E-19
V$LEF1_03	**LEF-1**	6,05E-17	17,56	10,6183	1,65	2,34E-15
V$KLF3_Q3_01	**KLF3**	6,50E-17	0,89	0,0153	58,5	2,34E-15
V$E2F1DP1RB_01	**Rb:E2F-1:DP-1**	4,24E-15	4,20	3,1908	1,32	1,38E-13
V$ZKSCAN1_04	**ZKSCAN1**	2,74E-14	23,08	13,1985	1,75	8,18E-13
V$IK_Q5_01	**Ikaros**	6,18E-14	0,85	0,0305	27,8	1,71E-12
V$E2F2_03	**E2F-2**	1,88E-13	1,35	0,1374	9,83	4,83E-12
V$CCNT2_01	**cyclinT2**	6,05E-13	13,73	8,2366	1,67	1,45E-11
V$XBP1_02	**XBP-1**	2,46E-12	13,97	8,3053	1,68	5,24E-11
V$EGR3_01	**Egr-3**	2,48E-12	2,46	0,458	5,37	5,24E-11
V$GMEB1_04	**GMEB1**	6,56E-12	1,79	1,5725	1,14	1,31E-10
V$EGR1_13	**Egr-1**	5,90E-11	10,77	3,4885	3,09	1,12E-09
V$PLAG1_01	**PLAG1**	6,48E-11	0,54	0,0076	71,0	1,16E-09
V$IK_Q5	**Ikaros**	9,30E-11	0,53	0,0076	70,0	1,59E-09
V$HIC1_02	**HIC1**	2,68E-10	0,56	0,0153	37,0	4,27E-09
V$BCL6B_04	**BCL6B**	2,74E-10	0,66	0,0305	21,5	4,27E-09
V$EGR1_11	**Egr-1**	4,19E-10	0,84	0,0687	12,2	6,27E-09
V$KLF3_Q3	**KLF3**	1,16E-09	0,48	0,0076	63,0	1,66E-08
V$NFAT_Q3	**NFAT**	1,63E-09	0,94	0,0992	9,46	2,26E-08
V$BCL11A_02	**BCL-11A**	1,84E-09	3,34	0,8321	4,02	2,45E-08
V$EGR1_09	**Egr-1**	4,87E-09	0,45	0,0076	59,0	6,03E-08
V$KLF_Q3	**KLF**	4,87E-09	0,45	0,0076	59,0	6,03E-08
V$TFIII_Q6	**TFII-I**	6,24E-08	0,49	0,0229	21,3	7,47E-07
V$SMAD5_Q5	**SMAD5**	9,16E-08	0,60	0,0458	13,0	1,06E-06
V$NFAT1_Q4	**NFATc2**	1,28E-07	1,13	0,1832	6,17	1,43E-06
V$ZF5_01	**ZF5**	5,73E-07	0,65	0,0687	9,44	6,23E-06
V$PRDM1_02	**PRDM1**	6,43E-07	0,58	0,0534	10,9	6,79E-06
V$IRF4_07	**IRF-4**	8,61E-07	0,43	0,0229	18,7	8,83E-06
V$HIF1A_Q6	**HIF-1alpha**	1,12E-06	1,51	1,1603	1,30	1,12E-05
P$AP1_01	**AP1**	1,44E-06	0,37	0,0153	24,5	1,40E-05
V$MEF2C_Q4	**MEF-2C**	2,58E-06	0,84	0,1298	6,47	2,43E-05
V$FOSL1_01	**Fra-1**	1,01E-05	4,55	2,7634	1,65	9,13E-05
V$SATB1_Q5_01	**SATB1**	1,02E-05	1,76	0,4351	4,04	9,13E-05
V$BEN_01	**BEN**	1,91E-05	1,22	0,2672	4,57	1,67E-04
V$SMAD1_Q6	**Smad1**	2,31E-05	1,65	0,4122	4,00	1,97E-04
V$EGR_Q3	**EGR**	2,41E-05	0,27	0,0076	35,0	2,01E-04
V$E2F_02	**E2F**	3,61E-05	3,38	2,0992	1,61	2,94E-04
V$CMAF_02	**C-MAF**	3,97E-05	10,81	5,8779	1,84	3,14E-04
V$EGR3_Q6	**EGR3**	4,02E-05	0,40	0,0382	10,6	3,14E-04
V$NFAT2_Q4	**NFATc1**	5,43E-05	0,76	0,1374	5,56	4,15E-04
V$EGR1_18	**EGR-1**	6,83E-05	0,24	0,0076	32,0	5,10E-04
V$RELBP50_Q3	**RelB:p50**	8,80E-05	1,63	0,4275	3,80	6,45E-04
V$ATF3_Q6	**ATF3**	1,07E-04	0,27	0,0153	18,0	7,69E-04
V$HIF2A_Q6	**HIF2A**	1,15E-04	1,62	1,1069	1,46	8,11E-04
V$EGR1_02	**EGR-1**	1,27E-04	0,37	0,0382	9,80	8,73E-04
V$EGR1_04	**EGR1**	1,76E-04	0,51	0,0763	6,70	0,0012
V$CREL_01	**c-Rel**	1,87E-04	0,30	0,0229	13,0	0,0012
V$HIF1AARNT_01	**HIF1A:ARNT**	2,10E-04	0,82	0,6336	1,29	0,0014
V$E2F2_04	**E2F-2**	2,20E-04	1,00	0,229	4,37	0,0014
V$REST_12	**REST**	2,24E-04	0,50	0,0763	6,60	0,0014
V$NR4A2_01	**NURR1**	2,60E-04	1,72	0,4809	3,57	0,0016
V$CMAF_Q5	**c-MAF**	2,92E-04	0,38	0,0458	8,33	0,0018
V$IRF2_01	**IRF-2**	3,17E-04	0,57	0,0992	5,77	0,0019
V$EGR2_01	**Egr-2**	3,28E-04	0,77	0,1603	4,81	0,0019

V$REST_06	**REST**	3,77E-04	0,31	0,0305	10,3	0,0022
V$MYB_Q5_01	**MYB**	4,54E-04	2,34	1,458	1,61	0,0026
V$IRF1_01	**IRF-1**	5,36E-04	0,20	0,0076	26,0	0,0030
V$FLI1_Q6	**FLI-1**	6,56E-04	1,58	0,4504	3,51	0,0036
V$RELA_03	**RelA-p65**	7,53E-04	0,19	0,0076	25,0	0,0041
V$NUR77_Q5	**NUR77**	8,13E-04	0,69	0,145	4,74	0,0044
V$NFKAPPAB_01	**NF-kappaB**	0,001134	0,25	0,0229	11,0	0,0060
V$REST_Q5	**REST**	0,0012	0,40	0,0611	6,50	0,0060
V$IRF7_Q3_01	**IRF-7**	0,0012	0,28	0,0305	9,25	0,0060
V$MYB_Q5_02	**MYB**	0,0012	2,24	1,3664	1,64	0,0061
V$HMGIY_01	**HMGIY**	0,0012	1,88	1,1756	1,60	0,0062
V$HIF1_Q5	**HIF1**	0,0014	0,51	0,4122	1,24	0,0067
V$TFIII_Q6_01	**TFII-I**	0,0014	0,34	0,0458	7,33	0,0068
V$TBP_Q6	**TBP**	0,0015	2,06	0,6489	3,18	0,0070
V$CREM_Q6	**CREM**	0,0015	0,62	0,4733	1,31	0,0073
V$SREBF1_02	**SREBP-1**	0,0017	3,89	1,374	2,83	0,0080
V$RELBP52_01	**RelB:p52 (NF-kappaB)**	0,0019	0,21	0,0153	13,5	0,0086
V$SOX5_07	**Sox-4**	0,0020	1,92	1,1832	1,63	0,0091
V$ASCL2_05	**Ascl2**	0,0021	0,17	0,0076	22,0	0,0093
V$HOXB2TBX21_01	**HOXB2:T-bet**	0,0022	0,24	0,2366	1,03	0,0098
V$EOS_01	**EOS**	0,0026	0,24	0,229	1,03	0,0114
V$REST_10	**REST**	0,0033	8,61	4,5038	1,91	0,0141
V$BEN_02	**BEN**	0,0034	8,34	4,3664	1,91	0,0146
V$NFKB1_Q4	**NFKAPPAB**	0,0036	0,22	0,0229	9,67	0,0153
V$ATF1_Q6_01	**ATF-1**	0,0040	0,60	0,4427	1,36	0,0166
V$RXRA_11	**RXR-alpha**	0,0041	0,89	0,2366	3,74	0,0166
V$RELA_Q6	**RelA-p65**	0,0041	0,50	0,1069	4,71	0,0166
V$PPARG_02	**PPARgamma:RXRalpha, PPARgam**	0,0041	13,24	6,7252	1,97	0,0166
V$HOXB2_01	**HOXB2**	0,0042	2,12	1,2595	1,68	0,0167
V$BCL3_03	**BCL-3**	0,0044	0,40	0,0763	5,30	0,0172
V$ZEB_01	**ZEB**	0,0046	1,15	0,3359	3,43	0,0180
V$ATF_01	**ATF**	0,0050	0,52	0,3893	1,33	0,0194
V$TCF7L2_06	**TCF-4**	0,0051	0,29	0,2519	1,15	0,0195
V$OCT_Q6	**Octamer**	0,0055	0,27	0,0382	7,00	0,0208
V$RARG_04	**RAR-GAMMA**	0,0056	0,15	0,0076	19,0	0,0210
V$CJUN_Q6	**C-Jun**	0,0058	2,94	1,6641	1,77	0,0210
V$CMYB_01	**c-Myb**	0,0058	0,67	0,4733	1,42	0,0210
V$SOX4_Q5_02	**Sox-4**	0,0058	0,67	0,1679	4,00	0,0210
V$CETS2_01	**Ets2 (c-ets-2)**	0,0059	3,14	1,7634	1,78	0,0212
V$ETS1_B	**c-Ets-1**	0,0060	0,24	0,0305	7,75	0,0214
V$CEBPB_01	**C/EBPbeta**	0,0061	0,89	0,2443	3,63	0,0215
V$HELIOSA_01	**Helios A**	0,0064	2,82	0,9924	2,84	0,0220
V$EGR1_12	**Egr-1**	0,0064	0,21	0,0229	9,00	0,0220
V$FOSBJUND_01	**FOSB:JUND**	0,0065	5,98	3,1679	1,89	0,0223
V$JUNBFRA1_01	**JUNB:FRA-1**	0,0073	12,86	6,4885	1,98	0,0247
V$MEOX1_02	**MEOX1**	0,0074	0,53	0,3893	1,37	0,0248
V$AHR_Q5	**AhR**	0,0075	0,25	0,2214	1,14	0,0248
V$ARNT_01	**Arnt**	0,0075	0,66	0,458	1,43	0,0248
V$JUN_04	**c-Jun**	0,0077	2,65	1,5038	1,76	0,0248
V$JUNBFOSB_01	**JUNB:FOSB**	0,0077	11,52	5,8397	1,97	0,0248
V$RELA_04	**RelA-p65**	0,0078	0,68	0,1756	3,87	0,0251
V$EFC_Q6	**RFX1 (EF-C)**	0,0080	0,46	0,3435	1,33	0,0255
V$STAT3_01	**STAT3**	0,0081	0,51	0,374	1,37	0,0256
V$POU6F1_02	**POU6F1**	0,0084	0,86	0,5649	1,51	0,0259
V$EBOX_Q6_01	**Ebox**	0,0084	0,20	0,0229	8,67	0,0259
V$PLAGL1_03	**Plagl1**	0,0084	0,20	0,0229	8,67	0,0259
V$JUNBFRA2_01	**JUNB:FRA-2**	0,0086	10,63	5,4046	1,97	0,0259
V$TATA_C	**TATA**	0,0086	0,17	0,0153	11,0	0,0259
V$MYB_03	**MYB**	0,0087	1,31	0,8092	1,62	0,0260
V$GABPAGABPB_Q6	**GABPalpha_GABPbeta**	0,0087	0,50	0,1145	4,33	0,0260
V$FOXO1_01	**FOXO1**	0,0089	1,27	0,3969	3,21	0,0260
V$NR4A2RXRA_01	**NURR1:RXR-ALPHA**	0,0089	0,66	0,458	1,45	0,0260
V$IRF8_Q6	**IRF-8**	0,0090	1,15	0,3511	3,28	0,0261
V$FLI1_03	**FLI1**	0,0091	2,71	1,5267	1,78	0,0261
V$MYBL1EOMES_02	**A-Myb:TBR2**	0,0092	0,36	0,2824	1,27	0,0262
P$ANAC042_01	**ANAC042**	0,0093	30,30	14,7099	2,06	0,0264
V$LEF1_04	**LEF-1**	0,0094	0,76	0,5115	1,49	0,0264

V$TP53_03	**TP53**	0,0095	1,80	1,0611	1,70	0,0264
V$TCF7L2_07	**TCF-4**	0,0097	0,20	0,1832	1,08	0,0266
V$ETV3_01	**ETV3**	0,0098	1,47	0,8855	1,66	0,0266
V$AP1_C	**AP-1**	0,0098	2,66	1,4962	1,78	0,0266

TRANSPARENT METHODS

Human CD4+ T cell isolation, activation, and differentiation. Human umbilical cord blood was layered on ficol (GE Healthcare, cat# 17-1440-03) for isolation of white blood cells. CD4+ T cells were then isolated using the bead-based CD4+ isolation kit from Invitrogen (cat# 11331D). For activation of T cells, a combination of plate-bound anti-CD3 (3750 ng/6-well culture plate well) (Beckman Coulter, cat# IM-1304) and soluble anti-CD28 (1 µg/mL) (Beckman Coulter, cat# IM1376) antibodies were used.

For Th17 cell culture, CD4+ T cells were stimulated as described above in a density of 0.5 × 10^6 cells/mL of X-vivo 20 serum-free medium (Lonza, Bazel, Switzerland). The X-vivo 20 media were supplemented with L-glutamine (2 mM, Sigma-Aldrich, Dorse, UK) and antibiotics (50 U/mL penicillin and 50 µg/mL streptomycin; Sigma-Aldrich). Th17 cell polarization was initiated with a cytokine cocktail of IL6 (20 ng/mL; Roche, cat# 11138600 001), IL1β (10 ng/mL, R&D Systems, cat# 201 LB) and TGFβ (10 ng/mL, R&D Systems, cat# 240) in the presence of neutralizing anti-IFNγ (1 µg/mL, R&D Systems, cat# MAB-285) and anti-IL4 (1 µg/mL, R&D Systems, cat# MAB204). For the control cells, CD4+ T cells were TCR stimulated with anti CD3 and anti CD28 in the presence of neutralizing antibodies without differentiating cytokines (Th0) and cultured in parallel.

iTreg differentiation was performed as described earlier (Ubaid Ullah et al., 2018). Briefly CD4+CD25- cells from multiple donors (three or more) were activated directly or pooled before activation with plate-bound anti-CD3 (500 ng/24-well culture plate well) and soluble anti-CD28 (500 ng /mL) at a density of 2× 10^6 cells/mL of X-vivo 15 serum-free medium (Lonza, Bazel, Switzerland). For iTreg differentiation, the medium was supplemented with IL-2 (12 ng/mL), TGF-β (10 ng/mL) (both from R&D Systems, Minneapolis, MN), all-trans

retinoic acid (ATRA) (10 nM) (Sigma-Aldrich), and human serum (10%, Biowest, cat# S4190-100) and cultured at 37°C in 5% CO2. Control Th0 cells were stimulated with plate-bound anti-CD3 soluble anti-CD28 in X-vivo 15 serum-free medium without cytokines.

Cell transfection with siRNA. Nucleofector 2b system (Lonza) was used for siRNA transfections. Four million cells were transfected in 100 µl volume of Opti-MEM (Gibco by Life Technologies, cat # 31985-047). After nucleofection cells were rested for 48 h in RPMI supplemented with 10% serum.

The following siRNAs (synthesized by Sigma or from Dharmacon) were used:

siNT 5´-AAUUCUCCGAACGUGUCACGU-3´ (Ubaid Ullah et al., 2018)

siCIP2A-1 5´-CUGUGGUUGUGUUUGCACU-3´ (Junttila et al., 2007)

Dharmacon siGENOME individual CIP2A siRNAs

siCIP2A-2: 5´-GAACAUAAGCUAGCAAAUU-3´

siCIP2A-3: 5´-GAAACUCACACGACUAUUU-3´

siCIP2A-4: 5´-GCACGGACACUUGCUAGUA-3´

siCIP2A-5: 5´-GUACCACUCUUAUAGAACA-3´

siAGK1 5´-AACAGAUGAGGCUACCUUCAG-3´

siAGK2 5´-GAGGCUACCUUCAGUAAGA-3´

siAGK3 5´-GGAGAGACCAGUAGUUUGA-3´

siPP2A 5'-TTTTCCACTAGCTTCTTCA-3'

Mice. CIP2A HOZ mice of C57BL/6 background were generated and provided by Prof Jukka Westermarck (Ventelä et al., 2012). The mice had leaky expression of CIP2A of

around 5% of the total. The permission for the mouse work was granted by the ethical committee of University of Turku for in vitro experiments of cells from mice.

Mouse CD4+ T cell isolation, activation, and differentiation. Mouse naive T cells were isolated from the spleen of mice (8-12 weeks) of the same gender. Spleens were macerated to prepare single cell suspension using a cell strainer and syringe plunger. Red blood cells were removed using ACK lysis buffer (Gibco by life technology, cat# A10492-01). CD4+CD62L+ T cells were isolated using a mouse CD4+CD62L+ T cell isolation kit (Miltenyi biotec, cat# 130-106-643) following the manufacturer's instructions. CD4+CD62L+ T cells were activated with anti-CD3, (1 μg/ml; BD Pharmingen, cat# 553238); and anti-CD28 (2ug/ml, BD Pharmingen, cat# 557393), both plate-bound. For the generation of Th17 cells, cells were stimulated in the presence of IL-6 (20 ng/ml; R&D, cat# 406-ML), TGF-β1 (1 ng/ml; R&D, cat# 240-B), IL1β (10 ng/ml; R&D, cat# 201-LB), anti-IL4 (10 μg/ml; BD, cat# 559062) and anti-IFN-γ (10 μg/ml; BD, cat# 557530). Cell culture experiments were performed in Iscove's modified Dulbecco medium (Sigma) supplemented with 5% (vol/vol) FCS, 0.002 M L-glutamine, non-essential amino acids (Gibco, cat# 11140-035), 100 U/ml of penicillin, 100 μg/ml of streptomycin and 50 μM β-mercaptoethanol (Gibco).

Flow cytometry. For surface staining, cells were stained with the antibody in FACS I buffer (1%FBS in PBS) at $+4^0$ C in dark for 15 min. Cells were then washed two times with FACS I, and finally re-suspended in FACS I Buffer or in PBS with 1% Formalin before acquisition in a BD LSR II/Caliber flow cytometer (BD Biosciences). For intracellular staining, cells were first fixed with 4% paraformaldehyde (PFA) for 15 min followed by resuspension in permeabilization buffer (10% saponin, 0.05% BSA in PBS) for 15 min on ice. Staining was performed for 1h. For Annexin (BD, cat# 556419)/PI (BD, cat# 51-66211E) staining, 24 h post cell activation, T cells were transferred, washed with PBS and resuspended in 50 μl

FACS1 buffer and 50 µl of 2X binding buffer (10mM Hepes; 140mM Nacl and 5mM Cacl2; PH7.4) with Annexin and PI. The data was acquired in the flow cytometer immediately after staining. For CFSE staining, cells were first washed and stained with CFSE (5 µM, Invitrogen, cat# C1157), then activated and cultured for four days before data acquisition. Data analysis was performed using Flowjo (FlowJo LLC) or flowing software (Version 2.5.1) (http://flowingsoftware.btk.fi/). The following antibodies were used for flow cytometry analysis: Anti-Mouse CD69 (eBioscience, cat# 11-0691-82), Anti-Human CD69 (BD, cat# 347823), Mouse IL17-PE (BD, cat# 559502), STAT3-PE (BD phosflow, cat# 557815), pSTAT3-AlexaFlour 647 (Y705; BD phosflow, cat# 557815).

TaqMan Quantitative Real-Time-PCR (TaqMan qRT-PCR). Cells were harvested, washed with cold PBS and lysed in RLT Buffer (RNeasy Mini Kit) containing β-mercaptoethanol. RNA was extracted using RNeasy® Mini Kit (Qiagen, cat #74106). DNA contamination was removed by on-column digestion using DNase (Qiagen cat # 79254) followed by in-tube DNase I digestion, (Invitrogen™, #18068-015).

The concentration of RNA was measured by UV absorbance using a Nanodrop 2000 detector (Thermo Fisher Scientific). For low RNA amounts (< 100ng) Roche Transcriptor First Strand cDNA Synthesis Kit (Cat# 04379012001) was used. Otherwise, for RNA amounts (100 ng - 1 µg) Invitrogen's SuperScript™ II Reverse Transcriptase (cat#18064-014) was used for cDNA Synthesis. For TaqMan qRT-PCR runs, cDNA was further diluted to 1:5 or 1:10. Using probes and primers designed by Universal ProbeLibrary System (Roche Life Science), TaqMan qRT-PCR reactions were run in QuantStudio™ 12K Flex Real-Time PCR System (Thermo Fisher Scientific). The data was analyzed using RQ Manager or Quantstudio software (Thermo Fisher Scientific). The threshold cycle (Ct) value

for the gene of interest was subtracted with an internal control (EF1alpha). The expression was then calculated as 2^{-dCt}.

Luminex assay. Cytokines in the supernatant were measured by Luminex assay (Milliplex MAP human/mouse cytokine/chemokine magnetic bead panel; Luminex 200 by Luminex xMAP technology) according to the manufacturer's instructions. The concentrations were normalized using cell count data obtained by flow cytometry.

Western Blotting. Cells were lysed in Triton-X-100 lysis buffer (TXLB) (50 mM Tris-HCl (pH 7.5), 150 mM NaCl, 0.5% Triton-X-100, 5% Glycerol, 1% SDS) and sonicated for 5 min using a Bioruptor sonicator (Diagenode). Protein concentration was then estimated using DC Protein assay (Biorad cat# 500-0111). Equal protein amounts were loaded onto acrylamide gel (Bio-Rad Mini or Midi PROTEAN® TGX precast gels). For protein transfer to PVDF membranes, mini or a midi transfer packs from Bio-Rad were used, depending on the gel size. Primary and secondary antibody incubations were performed in 5% Non-Fat milk or BSA in TBST buffer (0.1%Tween 20 in Tris-buffered saline). Quantification of the detected bands was performed using Image J software after normalization to the loading control. The following antibodies were used for western blotting: total STAT3 (Cell Signalling, cat# 9139), Phospho STAT3 (Y705) (Cell Signaling, cat# 9131), CIP2A (Junttila et al., 2007; Côme et al., 2016) Beta-actin (Sigma, cat # A5441), and AGK antibody (Abcam ab137616).

RNA sequencing. Total RNA was purified using RNeasy Mini Kit following the manufacturer's instruction. Libraries were prepared using the Illumina protocol. The quality of the library was confirmed using Advanced Analytical Fragment Analyzer (Advanced Analytical Technologies, Heidelberg, Germany) or with an Agilent Bioanalyzer, and the concentrations of the libraries were quantified with Qubit® Fluorometric Quantitation (Life Technologies, ThermoFisher). The sequencing was performed using a HiSeq2500 Next-

Generation Sequencing platform at the Finnish Functional Genomics Centre (FFGC). The quality control of raw sequencing reads was performed with FastQC, and adapters and low-quality bases were trimmed by Trimmomatic (Bolger et al., 2014). The trimmed reads were then aligned to the human reference genome GRCh37.75 (Ensembl release 75) using Tophat2 (Kim et al., 2013). HTseq-count (Anders et al., 2015) was used to calculate summarized read counts for each gene. The R/Bioconductor package edgeR (Robinson et al.,2010) was used to identify differentially expressed (DE) genes. Genes with a false discovery rate (FDR) < 0.05 were considered significantly DE.

IPA analysis. Pathway analysis was performed using Ingenuity Pathway Analysis (IPA) (https: www.ingenuity.com/, May 2016). P-values < 0.01 were considered significant. Key upstream regulators were also identified by IPA. Positive and negative z-score denote predicted upstream positive and negative regulators, respectively. Upstream regulators with p-value > 0.01 and |z-score| > 2 were considered significant.

Gene Set Enrichment Analysis (GSEA)

The gene set for the analysis were Th17 or iTreg signature genes, which were defined as those upregulated more than four-fold in respective conditions at 24h in the time series data (Tuomela et al., 2016). The enrichment in CIP2A-deficient RNA-seq data of 24h was calculated using GSEA tool (Subramanian et al., 2005). The parameters were as follows: Number of permutations: 1000; permutation type: phenotype; enrichment statistics: weighted; metric for ranking: Signal2Noise; gene list sorting: real. Signal2Noise metric uses the “difference of mean scaled by standard deviation”. Signal to noise ratio is defined as $(\mu A-\mu B)/(sA+sB)$ where μ is mean and s is standard deviation of samples A and B. The p-value cut-off used was 0.05.

Transcription Factor Binding Sites (TFBS) motif enrichment analysis.

The TFBS analysis was performed as described before (Ubaid Ullah et al., 2018). Briefly, we analyzed the promoters (-1000 to 100 bp from TSS) of 136 DE genes using the FMatch tool of the TRANSFAC database (Release 2018.2) and a custom profile of matrices corresponding to the TFs DE in human Th17 or iTreg cells (Tuomela et al., 2016; Ubaid Ullah et al., 2018). Binomial test was used to calculate enrichment. Benjamini & Hochberg method in r (version 3.4.3) was used to correct the p-value and FDR < 0.05 was considered significant.

Statistics and plotting. To determine the statistical significance of means, two-tailed paired or unpaired student's T-tests were performed, p-value < 0.05 was considered significant. For plotting, Microsoft Excel and R were used.

Immunoprecipitation (IP) and Mass Spectrometry (MS). For STAT3 and CIP2A pull-downs, an IgG-bound phospho-specific (Y705) STAT3 antibody and CIP2A specific antibodies were respectively used with an equivalent IgG antibody as control. The pull-downs were made using a Pierce™ MS-Compatible Magnetic IP Kit (Thermo Scientific, cat# 90409) as described below. Cells were harvested on ice and the culture medium was removed, followed by one wash with PBS. Cells were then re-suspended in ice-cold IP-MS Cell Lysis Buffer, as recommended by the manufacturer, and incubated on ice for 10 min with periodic mixing. The lysate was centrifuged at ~13,000 × g for 10 min to pellet the cell debris and the supernatant was transferred to a new tube for protein concentration determination. The cell lysates (500µg) were incubated overnight with 5µg of IP antibody. The antibody/lysate solution was diluted to 500 μl with the IP-MS Cell Lysis Buffer provided in the kit and incubated at $+4^0$ C with mixing overnight to form an immune complex. The immune complex was subsequently incubated with Protein A/G magnetic beads for 1h at

163 room temperature. The beads were then washed and target antigen was eluted with the IP-
164 MS Elution buffer. A Speed-Vac concentrator was used to dry the eluent, after which the
165 samples were prepared for proteomics analysis or analyzed by WB.

166 The IP samples from four biological replicates were denatured with urea, reduced, alkylated
167 and tryptic digested for proteomics analysis by LC-MS/MS. An EASY-nLC 1200 UPLC
168 system with a Q Exactive HF quadrupole – Orbitrap mass spectrometer was used. The data
169 analysis was made using MaxQuant with an inbuilt Andromeda search engine (Cox and
170 Mann, 2008; Cox et al., 2011). The mass spectrometry raw files were searched against a
171 UniProt human protein sequence database (version June 2016, 20,237 entries). The
172 database search parameter allowed one missed cleavage, cysteine carbamidomethylation
173 as a fixed modification and methionine oxidation as a variable modification. A false discovery
174 rate (FDR) of 0.01 at peptide and protein level was applied. MaxQuant's label-free
175 quantification (LFQ) algorithm was used to calculate the relative protein intensity profiles
176 across the samples (Cox J et al., 2014) The "match between run" option was enabled to
177 perform matching across the mass spectrometric measurements.

178 The LFQ protein intensity values (MaxQuant output) was further processed using the
179 Perseus statistics and informatics platform. Briefly the output was filtered to remove proteins
180 detected only by site, reversed hits, and contaminants and proteins detected with less than
181 two unique peptides (Cox et al., 2014; Tyanova et al., 2016). In the order of 850 proteins
182 were detected by two or more unique peptides, although after filtering for missing values
183 ~750 were suitable for the statistical comparison and used in the subsequent analysis. The
184 differences in relative abundance of the proteins detected in the pull-downs were evaluated
185 using a permutation-based t-test in Perseus.

The filtered LFQ protein intensities were analyzed using the Resource for Evaluation of Protein Interaction Networks (REPRINT) interface (Mellacheruvu et al., 2013). In brief, the average LFQ intensity was calculated from the triplicate analyses of each biological replicate of the IPs and the mock baits, and the data analyzed using the SAINT scoring algorithm to compare the variation and relative protein intensities. The data were then filtered to include proteins with the Significance Analysis of INTeractome (SAINT) score greater than 0.7.

Network analysis and Enrichment analysis. Known protein-protein interactions for the detected STAT3 interacting proteins were downloaded from the STRING functional protein association network database version 11 (Szklarczyk et al., 2017). Both predicted and experimental high confidence (interaction score $\geq$ 0.7) interactions were considered. The resulting network was visualized with Cytoscape version 3.7.1 (Shannon et al., 2003). Clusters in the network were identified using the Markov clustering algorithm executed in the Cytoscape plug-in clusterMaker v2 algorithm MCL Cluster (Morris et al., 2011) with the granularity parameter (inflation value) set to 1.8 as suggested by the previous work of Brohée & van Helden (Brohée and van Helden, 2006).

To define the strength of interactions of proteins with STAT3 in the two different conditions, SAINT probability scores (SP) were used. A new combined interaction SP score was calculated as: SP siCIP2A - SP siNT. While the individual SP scores range from 0 to 1, the combined SP score ranges from -1 to 1. A value of -1 corresponds to interactions with STAT3 only in the siNT condition, while a value of 1 corresponds to interactions with STAT3 only in the siCIP2A condition. A value of 0 corresponds to interactions with STAT3 that have equal strength in both conditions. The combined SP metric was color coded as a continuous gradient from blue (-1) to white (0) to red (1) for Figure 5D.

The enriched GO biological processes in the STAT3 interactome were identified using the Database for Annotation, Visualization and Integrated Discovery (DAVID) version 6.8 (Huang et al., 2009; Huang et al., 2009). The enrichment analysis was performed using the detected STAT3 interactome as the input and the whole detected Th17 proteome from our Th17 profiling study (Tripathi et al., 2019) complemented with the detected STAT3 interactome as the background reference. The GO FAT terms from DAVID were considered, which filter out the broadest, non-specific terms. For each cluster with more than four members, the most frequent enriched GO FAT biological process was identified. A biological process was considered enriched if it had an FDR ≤ 0.05.

Immunofluorescence and co-localisation. Th17 cells were plated onto acid-washed glass coverslips. 4 % PFA was used to fix the cells at room temperature (RT) for 10 min after which the cells were permeabilized in PBS containing 30% horse serum and 0.1% Triton X-100 for 10 min at RT, washed in PBS and then blocked in PBS-30% horse serum for 1h at RT followed by their incubation with primary antibodies overnight at 4°C. Next day, cells were washed three times using PBS and incubated for 1h at RT with AlexaFluor-conjugated secondary antibodies (Life Technologies). After three washes, cells were mounted with Mowiol for 30 min at 37°C. Images were taken with Carl Zeiss LSM780 laser scanning confocal microscope equipped with 100×1.40 oil plan-Apochromat objective (Zeiss). Corrected total cell fluorescence was calculated from confocal images to quantify the intensities in Th0 and Th17 cells and displayed as arbitrary unit (Burgess et al., 2010; McCloy et al., 2014). Co-localization of pSTAT3 with AGK was calculated from around 100 cells stained for STAT3 and AGK-positive cells in 7 different section views in the siRNA treated Th17 cells. The ratio of AGK colocalizing with STAT3 was calculated in both

conditions. Pearson correlation coefficients (PCC) were calculated to evaluate the statistical significance of the differences.

Selected reaction monitoring (SRM) mass spectrometry. Isotopically-labeled synthetic peptide analogues (lysine $^{13}C_6$ $^{15}N_2$ and arginine $^{13}C_6$ $^{15}N_4$) for AGK and CIP2A were obtained from Thermo Scientific. The peptides were analyzed by LC-MS/MS using a Q Exactive HF quadrupole – Orbitrap mass spectrometer (as above). Skyline software (MacLean et al., 2010) was subsequently used to select suitable transitions from the MS/MS spectra of heavy labelled peptides.

The validation samples were prepared using the same protocols used for pSTAT3 IP-MS. The samples were then spiked with synthetic heavy labelled analogues of the peptide targets and a retention time standard (MSRT1, Sigma) for scheduled selected reaction monitoring (SRM). The LC-MS/MS analyses were conducted using Easy-nLC 1000 liquid chromatograph (Thermo Scientific) coupled to a TSQ Vantage Triple Quadrupole Mass Spectrometer (Thermo Scientific). The column configuration was the same as used with the Q Exactive, although the peptides were separated using a modified gradient of 8% to 43% B in 27 min, then to 100% B in 3 min, at a flow rate of 300 nl/min (the mobile phase compositions are as indicate above). The raw SRM data, including other CIP2A associated targets, are available through PASSEL (Farrah et al., 2012) with the dataset identifier PASS01186.

Supplemental References

Anders, S., Pyl, P. T. and Huber, W. (2015) 'HTSeq--a Python framework to work with high-throughput sequencing data.', *Bioinformatics (Oxford, England)*, 31(2), pp. 166–9.

255 doi: 10.1093/bioinformatics/btu638.

256 Bolger, A. M., Lohse, M. and Usadel, B. (2014) 'Trimmomatic: a flexible trimmer for
257 Illumina sequence data.', *Bioinformatics (Oxford, England)*, 30(15), pp. 2114–20. doi:
258 10.1093/bioinformatics/btu170.

259 Brohée, S. and van Helden, J. (2006) 'Evaluation of clustering algorithms for protein-
260 protein interaction networks', *BMC Bioinformatics*. BioMed Central, 7(1), p. 488. doi:
261 10.1186/1471-2105-7-488.

262 Côme, C. *et al.* (2016) 'CIP2A promotes T-cell activation and immune response to Listeria
263 monocytogenes infection', *PLoS ONE*, 11(4), pp. 1–18. doi:
264 10.1371/journal.pone.0152996.

265 Cox, J. *et al.* (2011) 'Andromeda: A Peptide Search Engine Integrated into the MaxQuant
266 Environment', *Journal of Proteome Research*, 10(4), pp. 1794–1805. doi:
267 10.1021/pr101065j.

268 Cox, J. *et al.* (2014) 'Accurate Proteome-wide Label-free Quantification by Delayed
269 Normalization and Maximal Peptide Ratio Extraction, Termed MaxLFQ', *Molecular &
270 Cellular Proteomics*, 13(9), pp. 2513–2526. doi: 10.1074/mcp.M113.031591.

271 Cox, J. and Mann, M. (2008) 'MaxQuant enables high peptide identification rates,
272 individualized p.p.b.-range mass accuracies and proteome-wide protein quantification',
273 *Nature Biotechnology*, 26(12), pp. 1367–1372. doi: 10.1038/nbt.1511.

274 Farrah, T. *et al.* (2012) 'PASSEL: the PeptideAtlas SRMexperiment library.', *Proteomics*,
275 12(8), pp. 1170–5. doi: 10.1002/pmic.201100515.

276 Huang, D. W., Sherman, Brad T. and Lempicki, R. A. (2009) 'Bioinformatics enrichment
277 tools: paths toward the comprehensive functional analysis of large gene lists', *Nucleic*

278 *Acids Research*, 37(1), pp. 1–13. doi: 10.1093/nar/gkn923.

279 Huang, D. W., Sherman, Brad T and Lempicki, R. A. (2009) 'Systematic and integrative
280 analysis of large gene lists using DAVID bioinformatics resources', *Nature Protocols*, 4(1),
281 pp. 44–57. doi: 10.1038/nprot.2008.211.

282 Junttila, M. R. *et al.* (2007) 'CIP2A Inhibits PP2A in Human Malignancies', *Cell*, 130(1), pp.
283 51–62. doi: 10.1016/j.cell.2007.04.044.

284 Kim, D. *et al.* (2013) 'TopHat2: accurate alignment of transcriptomes in the presence of
285 insertions, deletions and gene fusions.', *Genome biology*, 14(4), p. R36. doi: 10.1186/gb-
286 2013-14-4-r36.

287 MacLean, B. *et al.* (2010) 'Skyline: an open source document editor for creating and
288 analyzing targeted proteomics experiments', *Bioinformatics*, 26(7), pp. 966–968. doi:
289 10.1093/bioinformatics/btq054.

290 Mellacheruvu, D. *et al.* (2013) 'The CRAPome: a contaminant repository for affinity
291 purification–mass spectrometry data', *Nature Methods*, 10(8), pp. 730–736. doi:
292 10.1038/nmeth.2557.

293 Morris, J. H. *et al.* (2011) 'clusterMaker: a multi-algorithm clustering plugin for Cytoscape',
294 *BMC Bioinformatics*, 12(1), p. 436. doi: 10.1186/1471-2105-12-436.

295 Robinson, M. D., McCarthy, D. J. and Smyth, G. K. (2010) 'edgeR: a Bioconductor
296 package for differential expression analysis of digital gene expression data.',
297 *Bioinformatics (Oxford, England)*, 26(1), pp. 139–40. doi: 10.1093/bioinformatics/btp616.

298 Shannon, P. *et al.* (2003) 'Cytoscape: a software environment for integrated models of
299 biomolecular interaction networks.', *Genome research*. Cold Spring Harbor Laboratory
300 Press, 13(11), pp. 2498–504. doi: 10.1101/gr.1239303.

301 Subramanian, A. *et al.* (2005) ‘Gene set enrichment analysis: A knowledge-based
302 approach for interpreting genome-wide expression profiles’, *Proceedings of the National*
303 *Academy of Sciences*, 102(43), pp. 15545–15550. doi: 10.1073/pnas.0506580102.

304 Szklarczyk, D. *et al.* (2017) ‘The STRING database in 2017: quality-controlled protein-
305 protein association networks, made broadly accessible.’, *Nucleic acids research*. England:
306 Oxford University Press, 45(D1), pp. D362–D368. doi: 10.1093/nar/gkw937.

307 Tripathi, S. K. *et al.* (2019) ‘Quantitative Proteomics Reveals the Dynamic Protein
308 Landscape during Initiation of Human Th17 Cell Polarization’, *iScience*, 11, pp. 334–355.
309 doi: 10.1016/j.isci.2018.12.020.

310 Tuomela, S. *et al.* (2016) ‘Comparative analysis of human and mouse transcriptomes of
311 Th17 cell priming’, *Oncotarget*. Impact Journals, 7(12), pp. 13416–13428. doi:
312 10.18632/oncotarget.7963.

313 Tyanova, S. *et al.* (2016) ‘The Perseus computational platform for comprehensive analysis
314 of (prote)omics data’, *Nature Methods*. Nature Publishing Group, 13(9), pp. 731–740. doi:
315 10.1038/nmeth.3901.

316 Ubaid Ullah, U. *et al.* (2018) ‘Transcriptional Repressor HIC1 Contributes to Suppressive
317 Function of Human Induced Regulatory T Cells.’, *Cell reports*. Elsevier, 22(8), pp. 2094–
318 2106. doi: 10.1016/j.celrep.2018.01.070.

319 Ventelä, S. *et al.* (2012) ‘CIP2A promotes proliferation of spermatogonial progenitor cells
320 and spermatogenesis in mice’, *PLoS ONE*. Edited by H. Clarke. Public Library of Science,
321 7(3), p. e33209. doi: 10.1371/journal.pone.0033209.

322